Article:

Skjærvø, SH, Marrows, CH orcid.org/0000-0003-4812-6393, Stamps, RL et al. (1 more author) (2020) Advances in Artificial Spin Ice. Nature Reviews Physics, 2. pp. 13-28. ISSN 2522-5820

https://doi.org/10.1038/s42254-019-0118-3

Contents

Title: Advances in Artificial Spin Ice

Sandra H. Skjærvø[1,2,*], Christopher H. Marrows[3], Robert L. Stamps[4], Laura J. Heyderman[1,2,*]

[1] Laboratory for Mesoscopic Systems, Department of Materials, ETH Zurich, 8093 Zurich, Switzerland
[2] Laboratory for Multiscale Materials Experiments, Paul Scherrer Institute, 5232 Villigen PSI, Switzerland
[3] School of Physics & Astronomy, University of Leeds, Leeds LS2 9JT, UK
[4] Department of Physics and Astronomy, University of Manitoba, Winnipeg, MB R3T 2N2, Canada

*corresponding authors

Abstract

Artificial spin ices, consisting of nanomagnets arranged on the sites of various periodic and aperiodic lattices, have opened a way to study a variety of fascinating phenomena such as frustration, emergent magnetic monopoles and phase transitions that, in the past, have mainly been the domain of bulk spin crystals and theory. Here we provide a review of recent progress in the field, beginning with emergent magnetic monopoles, which are mobile excitations with magnetic charge that have the potential to be exploited in future spintronic devices and can be constrained to move in particular directions. We then discuss the latest developments concerning thermally active phenomena, in particular the phases and phase transitions that can be observed for a selection of artificial spin ice geometries. Artificial spin ices also show promise as reprogrammable magnonic crystals and, with this in mind, we give an overview of the measurements of fast dynamics in these magnetic metamaterials. In terms of geometries, the focus was originally on elongated nanomagnets placed on the sites of the square and kagome lattices but, more recently, there has been a considerable increase in the diversity of designs. This has included altering the shape and size of the nanomagnets, the decimation or combination of known lattices, and rotation or multiplication of the nanomagnets at the sites of the lattices. In addition, quasicrystal lattices have been implemented and nanofabrication routes to produce artificial spin systems in three dimensions are being explored. Different magnetic materials can be incorporated, for example, to modify anisotropies and blocking temperatures. With this large variety, the way is open to discover startling new phenomena and we complete this review with possible directions for the future.

1. Introduction

Artificial spin ices are designer metamaterials in the sense that they are created from arrangements of single-domain dipolar-coupled magnets with nanoscale dimensions and exhibit a variety of properties, such as collective dynamics, not inherently present in their building blocks. The nanomagnets are arranged in such a way that the moments are frustrated, which means that not all dipolar interactions between the nanomagnets can be satisfied simultaneously. They were originally conceived [1] to mimic the behaviour of spins in their crystal counterparts, such as the rare earth titanate pyrochlores [2], which have spins positioned on the corners of tetrahedra. Correspondingly, the nanomagnets are placed on the sites of a square or kagome lattice (**Figure 1**). The mesoscopic size of the nanomagnets makes it possible to directly observe the moment configurations with magnetic microscopy techniques. Field-driven phenomena were at first the focus of interest, with observations of magnetization reversal as well as the use of an alternating magnetic field to perform an effective thermal anneal. Later it became possible to create thermodynamic systems where the energy barrier to switching was small enough to allow the moments of the nanomagnets to switch spontaneously, but in a collective manner mediated by the dipolar interaction between the nanomagnets. In the current review, we focus on what has happened in the field since the reviews in 2013 [3,4], which provide a useful foundation for the reader who is unfamiliar with the field.

In these frustrated arrangements of nanomagnets, there have been a wide variety of emergent phenomena discovered including emergent magnetic monopoles [5,6] (covered in **Section 2**), vertex based frustration [7,8], chiral dynamics [9] and phase transitions[10-12] (see **Section 3** and **5**). The existence of these emergent phenomena, which arise from the collective behaviour of the nanomagnets, underscores why artificial spin ices can be considered to be metamaterials. Artificial spin systems are also very important for high frequency dynamics because of their potential as programmable magnonic crystals [13], which is the theme of **Section 4**. Underpinning the research into artificial spin ice is the possibility with electron beam lithography to tailor the geometry at will providing “engineering by design”. This means that any arbitrary design can be realised, including more exotic arrays, not just based on extensions of the square and kagome geometries [7,14-16], but also going beyond periodic systems to artificial quasicrystals [17,18], which we cover in **Section 5**. In addition to systems with separated elongated nanomagnets, there are also noteworthy systems with circular [19-23] or square magnets[24], or connected systems where domain walls can travel through the network (relevant citations are given in the last paragraph of **Section 2** and in the subsection concerning magnonics in **Section 4**). We also mention the first efforts to create and characterize three-dimensional artificial lattices.

2. Emergent Magnetic Monopoles

The interest in magnetic monopoles in condensed matter systems was inspired by a publication in 2008, where Castelnovo, Moessner and Sondhi discussed the idea of mapping the dipoles in a spin ice system onto charge dumbbells [25]. Following this work, it was not long before the signatures of such monopoles were experimentally observed in the rare earth titanate pyrochlores [26-28] and the term "magnetricity" was coined [29] indicating that it might be possible to harness such magnetic charges in devices just as electrons and spins are exploited in electronic and spintronic devices.

It was then a natural step to consider how emergent magnetic monopoles would behave in the corresponding artificial spin ices (see description of emergent magnetic monopoles in **Box 1**). In 2009, the first discussion of emergent magnetic monopoles in artificial spin ice appeared [30], theoretically considering interactions between charge excitations in artificial square ice, which not only have a Coulombic interaction but also a confining potential, or string tension, binding the charge defect pairs. Shortly afterwards, the first experimental observations of the creation and separation of monopole-antimonopole pairs in an applied magnetic field, leaving behind them strings of reversed magnets referred to as Dirac strings, were reported in disconnected [6] and connected [5] artificial kagome spin ice. In the disconnected system, the Dirac strings were found to be one-dimensional while, in the connected artificial kagome spin ice, branching was observed. This highlights the fact that the behaviour during magnetization reversal is sensitive to the local energetics, which in turn are highly dependent on the detailed geometry of the artificial spin ice [31]. Indeed, one of the appeals of artificial spin ice is that the behaviour can be tuned through the lattice type and parameter, as well as nanomagnet shape and size. Furthermore, viewing artificial spin ice in terms of emergent magnetic monopoles also provides a means to visualise the inherent physical phenomena. For example, in an artificial square ice, mapping of the behaviour of magnetic monopoles during magnetization reversal gives important insights into memory effects at the microscopic level [32].

The first direct observation of the spontaneous creation and separation of charge defects, or Type III vertices (for vertex types, see **Figure 1**), in a thermally-active artificial square ice was reported in 2013 [33]. On separating, the defects left behind strings of reversed magnets against a Type II vertex background (**Figure 2a-f**). Here, an applied magnetic field was used to set the initial remanent state of the sample with all vertices in a Type II configuration and the authors pointed out that the interaction energy between the charges, attractive or repulsive, is dependent on the background configuration. In a thermally-active artificial kagome spin ice, it was found that the emergent magnetic monopoles remain confined, since increasing the length of the strings beyond one spin flip is energetically unfavourable [34]. Therefore, important in defining the behaviour of the monopoles are both the background magnetic configuration and the artificial spin ice geometry, which can be modified by introducing defects into the lattice [35-37]. Interestingly, the string tension can be exploited in artificial square ice to obtain spontaneous magnetic currents, first stretching the bound monopoles apart with an applied magnetic field and removing the field in order to release them, and it was suggested that this effect may be of interest for energy storage [38].

As the charge defect (Type III vertex) pairs in thermally-active artificial square ice continue to be created and spread through the system, the strings eventually coalesce to form domains of ground state vertices separated by Type II boundaries (**Figure 2 g,h**). Charge defects in the form of

Type III vertices can propagate along the domain boundaries providing a mechanism for them to decrease in length until they disappear [33,39].

Even though the string tension between two monopoles decreases with increasing distance between them, an important question to answer is whether it is possible to create an artificial square ice where the string tension is absent to give truly unconfined emergent magnetic monopoles that interact via a Coulomb interaction only. The key to this issue is the fact that the four nanomagnets at a vertex do not have equivalent interactions since the intermagnet separations and angles are not the same. One possible solution is to raise one sublattice with respect to the other [40-44] so that, at a critical vertical separation, the so-called Coulomb phase is achieved [45], with emergent magnetic monopoles freely moving in a highly degenerate, divergence-free background. Another possibility to reduce the string tension is to use two different sublattice parameters [46,47]. In lattices of connected elements, modifying the size and shape of the vertex, for example by fabricating a hole at the vertex centre or making the elements thinner, can also make the Type I and Type II vertices similar in energy [48,49]. In this regard, measurements of the magnetic susceptibility can give helpful information on both the monopole motion [50] and the charge correlation length associated with monopoles [51]. Another valuable signature of monopole defects and their Dirac strings appears in the frequency spectrum [52-54], which provides a macroscopic means of identifying monopole defects where the spectral amplitude is proportional to the number of defects. Indeed, artificial spin ices are interesting candidates for reconfigurable or reprogrammable magnonic crystals, which we discuss further in **Section 4**.

Going to geometries beyond the square ice, one would expect a very different behaviour of the effective charges [14]. For example, in the shakti lattice [7], it is possible to see signatures of charge screening involving magnetic monopole polarons analogous to polarons associated with electrons in a crystal [55]. These magnetic charges emerge at the four-magnet vertices in the shakti lattice, which are surrounded by three-magnet vertices that, due to their topology, will always have magnetic charge. By careful design, it is also possible to control the emergent magnetic monopoles, which is important for device applications. For example, charge defects can be constrained to move in particular directions using certain geometries [56] or a temperature gradient [57], and they can also be controlled by locally inducing strain with an electric field [58].

This Section would not be complete without mentioning that magnetic domain walls within the nanowires constituting connected artificial spin ice systems can also be considered as charge carriers [59]. These walls are chiral objects where the magnetization within the wall rotates either clockwise or anticlockwise, independent of whether the lattice itself has chiral symmetry. Interestingly, when the walls approach a Y-shaped vertex in an artificial kagome ice on application of a magnetic field (**Figure 2 i,j**), this domain wall chirality can determine whether they will move into the left or the right branch [60,61]. Taking advantage of this, a domain wall passing through tailored Y-junctions, which are the basic unit of connected artificial kagome spin ice, can be used to perform logic operations [62,63]. However, care needs to be taken since the walls may transform into domain walls of opposite chirality for particular fields and geometries [64,65], and the propagation behaviour of domain walls depends on the magnitude and orientation of the applied magnetic field [66-68]. To circumvent these effects, the geometry of the Y-junctions can be modified so that the symmetry of the branches is reduced, giving a deterministic domain wall path that is independent of DW chirality [69]. It is also possible to nucleate domain walls in particular positions in connected artificial spin ice using a magnetic tip, thereby creating specific magnetic configurations at will [70]. Finally, we note that, just as the chirality of the domain walls provides additional degrees of freedom in connected artificial spin systems, the edge bending of the magnetization at the vertices in disconnected lattices also gives an additional chiral degree of freedom to the vertex monopoles [71] (**Figure 2k**).

3. Thermodynamics and kinetics

Thermally active artificial spin systems. Since the beginning of the field, it has been of fundamental interest to understand the collective behaviour of the nanomagnets in artificial spin ices, in particular how they access thermodynamically favourable magnetic phases. The first experimental observations of a magnetic phase transition in an artificial spin system was on the square geometry, where magnetization measurements indicated a decrease in macrospin order well below the intrinsic ordering temperature of the nanomagnet material[10]. Nevertheless, for other geometries it has been a challenge to fabricate arrays of nanomagnets that remain thermally active down to temperatures where their magnetic moments are predicted to thermodynamically order as a result of the dipolar interactions. Here we give an overview of the earlier efforts using thermal annealing and field protocols before reviewing the advances that finally lead to the flourish of work on truly thermally active artificial spin ices.

The earliest examples of artificial spin ice were athermal at the temperature of the experiments, which were conducted at room temperature. For these athermal systems, effective thermodynamics were probed using applied alternating magnetic fields, for which an effective temperature [72,73] and effective entropy [74] were defined. Thermal ordering in these artificial spin systems could only then be achieved by annealing the samples above the Curie temperature, T_C [75-77]. Indeed, such thermal protocols proved to be more effective for lowering the residual entropy of the system than the previously used field protocols for athermal systems [1,78,79].

In a thermally-active artificial spin system, a nanomagnet is considered to be thermally active if the time taken for the measurement, t_m, is longer than the time required for the moment of a nanomagnet to switch, t_s, which is described by the Arrhenius law:

$$\frac{1}{t_s} = \frac{1}{t_f} e^{-\frac{KV}{k_B T}} \qquad (1)$$

where $1/t_f$ is the attempt frequency, V is the magnetic volume of the nanomagnets, k_B is the Boltzmann constant and K is the anisotropy constant that is related to the shape of the nanomagnets and is given by $K = \frac{1}{2} \mu_0 M_S^2 \Delta N$ for ellipsoids [80], where μ_0 is the magnetic permeability of free space, M_S is the saturation magnetization and ΔN is the difference between the demagnetizing factors along the in-plane short and long axes of the nanomagnets [81]. We can define the 'blocking temperature', T_b, as the lowest temperature where the nanomagnets appear to be thermally active, or superparamagnetic (or perhaps more correctly 'paramagnetic superspins') at the timescale of the measurement ($t_m < t_s$). Below T_b, the energy required to switch the magnetic moments is higher than the thermal energy, and the nanomagnets will appear to be frozen with static magnetic moments at the timescale of observation. For nanomagnets in artificial spin ice, the switching has been shown to occur through a nonuniform process[82], leading to a much lower T_b than is expected for magnets displaying single-domain coherent rotation, for which Equation 1 applies. The moments of an artificial spin ice comprising weakly coupled nanomagnets have further been shown to freeze in similar manner to that of a glass on approaching T_b from above, where the system crosses over from the thermally equilibrated state to the frozen state following a Vogel-Fulcher-Tammann law [82,83].

To observe thermally active behaviour in artificial spin ice, the blocking temperature T_b needs to be below the temperature of the experiments that are ideally performed close to room temperature. For this, Equation 1 provides some insight into how to lower the blocking temperature T_b by modifying the individual nanomagnets, despite the fact that it does not fully reflect the switching mechanism of the nanomagnets. Firstly, the nanomagnet volume can be decreased by reducing the thickness and/or the lateral dimensions of the magnets [33,84,85]. Secondly, the shape anisotropy, K, of the magnets can be reduced by lowering the aspect ratio (nanomagnet length relative to width) or the magnetization of the nanomagnets. Thirdly, the magnetization of the magnetic material can be lowered. Typically, artificial spin ice is manufactured from ferromagnetic elements fabricated from Permalloy, a soft magnetic alloy that has a composition close to 80% Ni / 20% Fe. Therefore, in order to reduce the magnetization of the Permalloy, the Ni content can be increased, thus lowering the Curie temperature T_C of the material [75]. Another possibility to reduce the magnetization is to alloy the magnetic elements with non-magnetic elements, such as palladium [77,86], or to use a ferrimagnetic material instead of ferromagnetic material [87].

One important aim is then to observe magnetic ordering in thermally active artificial spin ice. For this, the nanomagnets need to be thermally active below the temperature of the respective phase transition(s). However, all of the routes to lower T_b involving a modification of the individual nanomagnets also simultaneously lower the transition temperature. This is because all such modifications (directly or indirectly) reduce the dipolar coupling between the nanomagnets, which is proportional to m^2/d^3. Thus, increasing the centre-to-centre distance d between the nanomagnets or decreasing the nanomagnet moment $m = M_S V$ will reduce both the T_b and the phase transition temperature. To counteract this effect on the transition temperature, and ensure it is above T_b, one can minimize the lattice parameter [76,85], which in turn decreases the nanomagnet separation, so giving an increase in the coupling between the nanomagnets. Therefore, great care in both the design of artificial spin systems and the thermal protocol is required to ensure that the system reaches equilibrium, especially at lower temperatures, and a useful discussion on determining whether a system is out-of-equilibrium can be found in a recent colloquium by Rougemaille and Canals [88].

Phases and phase transitions. The progress in fabrication, allowing the manufacture of artificial spin systems with spontaneously fluctuating moments, fuelled the research for studying the collective behaviour in thermally-active artificial spin systems. We review here the latest findings regarding the prototypical square and kagome lattices, before we touch on the more exotic and still rather unexplored lattices.

The predicted ground state in artificial square ice [42] was experimentally verified in 2011 in samples that ordered during the early deposition of the Permalloy film from which they were made [89]. The ordering was later reproduced using thermal annealing protocols [75-77] and observed in thermally active systems [33]. This ordering is a result of the fact that, while all ice-rule obeying vertex configurations have low energy, the non-equal interactions between the nanomagnets at the vertices lift the degeneracy, favouring the lowest energy Type I vertices [1]. As a result the non-equal interactions at the vertex, the artificial square system does not have an extensive degeneracy, and has been theoretically suggested to belong to the two-dimensional Ising universality class with a continuous phase transition[90,91]. In recent X-ray scattering experiments, the first measurements of critical behaviour across the phase transition have been obtained, providing evidence of a continuous two-dimensional Ising transition[12]. In addition, it may be possible to alter the nature of the phase transition by modifying the energies of the vertex configurations, for example using an exchange bias field[92].

One of several ways to equalize the intermagnet interactions in the square ice geometry is to lift the nanomagnets on one of the two sublattices out of the plane (**Figure 3a**) [40-42], which has been experimentally realized [43,44]. While the structure factor deduced from the MFM images of conventional square ice displayed the expected peaks associated with ordering (**Figure 3b**), 'pinch points' emerged in the structure factor for the fully degenerate square ice (**Figure 3c**). These pinch points are a signature of a so-called Coulomb phase [45], which obeys Gauss' law and supports magnetic monopole excitations that emerge in highly frustrated systems. The same effect is predicted to be achieved in a purely two-dimensional system in which the interactions at the vertices are tuned by connecting the nanomagnets having made appropriate choices for their width and thickness[48].

It is predicted that the artificial kagome spin ice, despite the extensively degenerate configurations arising from the geometrical frustration, has a rich phase diagram, including a long range ordered phase, due to the presence of long-range dipolar interactions between the nanomagnets [42,93]. The predicted phases are shown schematically in **Figure 3d.** On cooling, there is first a crossover from a disordered paramagnetic phase to another paramagnetic phase, referred to as kagome ice I, in which the ice rule is obeyed with magnetic charges of +1 or -1 at each vertex. The cooperative paramagnetic behaviour of the kagome ice I phase means that it can be seen in the framework of spin liquid physics[88]. A spin liquid is a disordered, but correlated magnetic state, in which the interactions within the assembly of classical Ising variables lead to pairwise non-zero spin correlations, but decay to zero at large distances. It is, however, important to note that the nanomagnets in artificial spin systems are only Ising-like, firstly because they have a finite size and shape with non-uniform magnetization, and, secondly, because they interact magnetostatically beyond their nearest neighbours. Upon lowering the temperature further, the system goes through two other phase transitions, first an Ising transition to the kagome ice II phase with ordered charges, but still with highly fluctuating moments, and then a transition to a long-range ordered phase with both charge and spin order. This last transition is a second-order three-state Potts transition, although simulations will give a Kosterlitz-Thouless transition if charge order-breaking fluctuations are not present[93,94]. Large system sizes are needed to observe the three-state Potts universality because these fluctuations have a very large correlation length[93]. Intriguingly, the emergence of the charge-ordered phase is not easily explained, as no charge degree of freedom is encoded in the underlying dipolar spin Hamiltonian[88,95]. The emergence of the charge order and the rest of the phase diagram can, however, be understood in terms of fragmentation of the spins into two parts; a divergence full part, which gives a static signature of ordered magnetic charges, and a divergence free part reflecting a disordered magnetic phase with fluctuating moments characteristic of a Coulomb phase [95-97]. The kagome ice II phase can thus be regarded as a spin liquid superimposed on a magnetic charge crystal.

In early studies, the difficulty of obtaining ordering in artificial kagome spin ice structures with sizes beyond four rings was demonstrated[84,98]. Regarding extended kagome lattices, indications of two phase transitions have been observed with muon rotation spectroscopy [11] and the first signatures of the relevant phases have been observed with neutron scattering and resistivity measurements performed on connected artificial kagome spin ice [99-102]. However, only small areas of the charge-ordered phase have been directly observed with imaging techniques following annealing [76,77,103], and the long-range ordering of the charge (spin ice II phase) or the spins (the ground state) have not yet been unambiguously observed. The difficulty in achieving ordering in the artificial kagome spin ice is due to the high frustration and extensive degeneracy of the system. Achieving the ground-state in such a degenerate energy landscape simply takes a very long time, which may also be hindered by kinetic restrictions. For example, it can be seen that, during ordering of the charges into the kagome ice II phase, domains with an even number of vertices are favoured. This indicates that two vertices with opposite charge prefer to order simultaneously so that charge neutrality is maintained, thus creating restrictions in how the domains grow [87]. Another challenge associated with achieving the ground state in highly frustrated systems is that they are very susceptible to external fields, which can dramatically change the energy landscape [104].

As we show in **Section 5**, there are many more geometries to consider beyond the kagome and square geometries. For more exotic lattices, it was found that the low energy states adopted by the extended system could not be predicted by considering the relative energies of the building blocks consisting of only a few nanomagnets [18,105]. Going beyond Ising-like systems to dipolar XY systems with arrays of coupled discs, complex ordering phenomena have been observed [19,20,22], and the phase diagrams of such XY systems can be modified by structural disorder to give new phases that favour local flux closure [20]. Both the lattice and the moment orientations define the ordering behaviour. For example, the kagome Ising system with out-of-plane moments displays behaviour that is quite different from its topologically equivalent kagome lattice with in-plane moments[88,106,107]. Furthermore, competing ferro- and antiferromagnetic orders have been observed in the quadrupolar ice. [108] Here pairs of elongated nanomagnets representing Ising moments are arranged in a similar manner to the individual nanomagnets in chiral ice and can be considered to be an array of quadrupoles (**Figure 3e-h**) (see **Section 5** for more details about the chiral ice). This system also provides a way to realise the Potts model, which has also been achieved by exploiting magnetocrystalline anisotropy in epitaxial thin films [24], and the competing interactions present result in a complex phase diagram dependent on field and temperature.

4. Fast dynamics

Resonances and spin wave excitations. Since the nanomagnets in artificial spin ices are typically manufactured from soft magnetic metals such as Permalloy, the magnetic resonances and spin wave excitations typically investigated occur in the 1-100 GHz range. When the artificial spin ices are made up of disconnected magnetic elements, the spin wave excitations can exist within each individual nanomagnet, appearing as modes of precession that can be strongly affected by the element shape, applied magnetic field direction and stray field from neighbouring elements [109]. Examples of standing and localised modes within an elongated, rectangular nanomagnet are depicted in **Figure 4a**, with the corresponding frequencies given in **Figure 4b** as functions of an external magnetic field applied along the direction shown [110]. The resonances here are mostly localised towards the edges of the rectangular nanomagnet. In addition, probing spin wave resonances for a static magnetic field applied at different angles gives valuable information [54], for example, allowing the identification of resonances from sets of magnetic elements with particular orientations.

Collective excitations in artificial spin ice have been predicted and studied for several geometries. In particular, the relationship between the lattice geometry, the magnetic configuration present and the resonant modes that occur within the nanomagnets has been demonstrated with experimental measurements on artificial square ice, which revealed multiple modes in the spectra in addition to the main resonance [111]. With micromagnetic simulations [112] and scaling arguments [51] it was shown that the modes can be understood in terms of number and position of emergent magnetic monopoles at the vertices, which in turn depends on the strength and direction of the applied field. In particular, the emergent magnetic monopoles created during reversal processes (**Figure 4c**) can be detected using ferromagnetic resonance (FMR) that, with its sensitivity to local fields, provides a way to distinguish contributions from different vertex types in the spectra [113,114]. The frequency spectrum for the artificial square ice in the low field region shown in **Figure 4d** reflects the generation of pairs of oppositely charged Type III vertices separated by a string of magnets with reversed moments as shown in **Figure 4c** [52]. From these spectra it is possible to identify features related to the string length and the number of defect pairs. The amplitudes of the spectra, for example, are related to the length of strings, while the frequencies are related to the location of the defects relative to the nanomagnet array boundaries. The magnetic configurations therefore have tell-tale signatures associated with the distribution of local fields acting on the associated elements [52].

Signatures in the resonant spectra can also arise from the non-uniformity of magnetization within the individual nanomagnets. In particular, sufficiently large elements will minimize their stray field energies with a canting of spins near the element ends [115]. This canting modifies the energy of resonances because of the additional possible configurations at the vertices. For example, for a Type I vertex in an artificial square ice (see **Figure 1a**), there are two possible canting directions at a vertex for each element, which results in two additional degenerate configurations [115].

Investigations of spin wave resonances in frustrated artificial spin systems are not just restricted to Ising-like systems. For example, coupled magnetic vortices arranged in a kagome geometry [116] , display collective oscillation modes of the interacting vortex cores that are sensitive to the application of an external magnetic field. This system is particularly interesting due to frustration that leads to multiple configurations for the vortices reflected by the resonant frequencies.

Magnonic crystals. In addition to using spin waves as a means to study defect formation in frustrated systems, artificial spin ice geometries may offer a platform for programmable spin wave devices[3]. In this regard, detection of spin waves in artificial spin ice with spin torque spectroscopy may be especially useful [117]. A connected geometry able to transmit spin wave information through a lattice is particularly suited for modification and control the spin wave manifold of states[118]. This concept is widely used for control of optical excitations in photonic crystals with patterned structures designed to diffract optical waves at certain wavelengths. The analogous patterned materials for spin waves are referred to as magnonic crystals and metamaterials, and there is a large body of work on the topic of magnonics and magnonic devices, of which composite and three-dimensional materials are possible future directions [13]. The concept of controlling spin wave band gaps and properties by adjusting interactions between active elements are being explored [119-121]. In artificial spin ice, this can be achieved with end canting[115], as discussed earlier in **Section 2**, and engineering interactions using interface induced chiral symmetry breaking. In addition, a periodic artificial spin ice geometry can be used to create a spin wave band structure where the frequencies near the zone centre can be tuned by setting the magnetic configuration [122]. The introduction of Dzyaloshinskii-Moriya chiral symmetry breaking in artificial spin ice is also of interest for magnonic device applications to give nonreciprocity as well as topologically protected spin waves in the long wavelength limit [123].

Difficulties with using nanometre scale magnetic elements for magnonic applications can arise simply because the material volumes are small. This can result in weak coupling between elements and signal-to-noise issues. Therefore, the material volume can be maximised by creating an array of holes in a magnetic thin film [124] often referred to as antidot arrays [125]. Here, instead of creating magnetic elements out of continuous films, one instead etches vacancies in the films with the desired shape, which can be left empty or filled with another material[126]. The vacancies create patterns in the local magnetic fields generated by the surrounding material, and define the magnetic environment controlling spin wave propagation. For example, in an array of elliptical holes arranged in an artificial square ice geometry that was characterised with Brillouin light scattering [127], a magnonic band structure was observed as well as a type of spin wave channelling. Another key aspect of such connected geometries is the possibility to transmit shorter wavelength exchange-dominated spin waves through the junctions connecting the elements [13,128]. The example shown in **Figure 4e-g** on connected artificial kagome spin ice [54] demonstrates how signatures from monopole resonances can be obtained for a two-step magnetization reversal process driven by a magnetic field applied along different lattice directions.

5. Further geometries and associated phenomena

One of the main attractions of the artificial spin ice approach is that novel phenomena can be observed in nanomagnet arrays where every aspect can be engineered with various nanofabrication methods. In this section, we discuss a broad range of artificial spin systems, many of which go beyond artificial spin ice, as they all share the philosophy of generating new emergent phenomena arising from the collective behaviour of constituent building blocks. We illustrate a selection of artificial spin systems and their relationships in **Figure 5** based on geometries that have been implemented to date. Indeed, the only limitation on possible designs is the imagination of the designer and, in this sense, artificial spin ices are examples of designer metamaterials. For example, it is possible to deliberately introduce lattice defects such as an edge dislocation in the artificial square ice, which is a topological defect in the structure (**Figure 6a**) and results in the creation of domain boundaries between areas of Type I ground state order that have one end pinned at the defects [37].

One of the first alternative lattices to the kagome and square geometries was the 'brickwork' lattice [129], which keeps the long axes of the nanomagnets orthogonal to each other, just as for square ice, but reduces the number of nanomagnets meeting at each vertex to three, making it topologically equivalent to the artificial kagome spin ice. However, since the lattice is not frustrated, its properties are more similar to the square than kagome spin ice. This demonstrates that the details of the geometry and symmetry are important in artificial frustrated systems, and they cannot be classified on topology alone.

As shown in **Figure 1**, the standard four vertex types of the square ice have a particular hierarchy of energies. This hierarchy can be modified in order to increase the frustration in the lattice. One example of tuning the hierarchy was to stretch the lattice to a rectangular shape so that increased degeneracy was achieved [46,47]. In another example, the introduction of magnetic nanodiscs into the gaps at the vertices [21], so-called 'slave' macrospins, was shown to equalize the energy between Type I and Type II vertices. The macrospin of the 'slave' discs is XY-like and therefore its direction is dictated by its magnetostatic interactions with the four elongated nanomagnets that surround it at the vertex. At a critical disc size, there is no longer an energy gap between the Type I and Type II vertex configurations, and pinch points are observed in the magnetic structure factor, indicating that the degeneracy of the ice-rule-obeying vertices has been restored. It is also possible to tune vertex energies by modifying the vertex shape and size in systems of connected elements by inserting a hole at the centre of the vertex or decreasing the width of the elements[48,49]. These approaches are easier in terms of fabrication compared to the approach of offsetting one of the sublattices out of the plane as discussed in **Section 3** and shown in **Figure 3a**.

The dipolar trident system is also based on the square ice in which the vertex configuration energies can be tuned. Here, each element in a square ice is reproduced to give a group of three parallel nanomagnets, which then interact among themselves [130]. These interactions modify the energies of the different vertex types that can be adjusted by modifying the distances between the three elements in the group and between the groups.

The trident lattice has an inherent chirality arising from the geometry of the trident design. In addition, a dynamic chirality was observed in the pinwheel system [131,132] referred to as a chiral ice [9], where the nanomagnets in a square ice are rotated through 45° (**Figure 6b**). Here, minimisation of the stray field energy at the edges of the array results in an unexpected ratchet effect in which thermal relaxation leads to a rotation of the magnetization of the array in a unique direction defined by the edge structure. The chiral ice has also been shown to prefer specific ferromagnetic ordering on tuning both the anisotropy of the system and the topology of its edges [131], and this leads to the appearance of flux closure states similar to the those found in mesoscale thin film patterned elements. Further geometries incorporating chiral plaquettes are the square-kite tessellation[105] and the vortex ice, which is based on the artificial kagome spin ice and results in a defined chirality of the vortex states in the hexagonal rings of nanomagnets [133]. Handedness in the magnetic order has also been observed in an artificial magnetotoroidal crystal, where the toroidal moment can be defined with the magnetic tip of an MFM [134]. In this geometry, the nanomagnets are arranged in squares that are repeated across the array, which is equivalent to replacing each element in artificial square ice with two elements (see also ref. [124] and supplementary information in ref. [135]). Hence, the lattice geometry is non-chiral, but the magnetic configuration is. Similarly, edge bending occurring at +3/-3 charged monopoles in the kagome lattice, shown in **Figure 2k,** adds magnetic chirality to an otherwise non-chiral lattice geometry.

It is possible to make different vertices play different roles by designing them to have different coordination numbers i.e. the number of nanomagnets meeting at a vertex. The pentagonal lattice [55] is an example of this class of lattices that possess a mixed coordination number, since it has either four or three nanomagnets meeting at each vertex. Mixed coordination number lattices not only house emergent magnetic monopoles, but also associated emergent magnetic polarons. Such screened charges have also been directly visualised as a transient state in dice lattice artificial spin ices, which has vertices with coordination of three or six [16].

Allowing mixed coordination numbers permits the construction of many more lattices, including the shakti, tetris, and Santa Fe lattices [8]. The most heavily studied of these is the so-called shakti lattice, constructed by removing elements from the square ice system in such a way that there is a mixture of coordination numbers 3 and 4 (**Figure 6c**). This decimated square ice has been shown theoretically to possess a quasicritical ice phase with critical correlations similar to those found in the Coulomb phase of the pyrochlore spin ices [136]. Artificial spin ices based on the shakti lattice have also been experimentally realised in both static [7] and thermally active [137] forms. In this class of vertex models, the frustration does not arise from the properties of an individual vertex, but rather from the inability of neighbouring vertices to take up their lowest energy configuration at the same time. The phenomenon is known as topologically-induced emergent frustration [7], which can only be realised with artificial spin systems since they have no known analogues in nature, and remains a fruitful avenue for future work. A modified version of the shakti lattice in which some of the nanomagnets are longer than the others has been shown to order differently due to the difference in switching barriers for the different nanomagnets [137]. Combining designs with different density and connectivity, for example in the tetris lattice [15], can also give rise to regions with different energy barriers as well as reduced dimensionality.

In addition to Ising-like systems, it is possible to create so-called dipolar-coupled XY systems from circular nanomagnets with stripe ordered low energy states [19,22], and introduction of positional disorder in such artificial spin systems modifies the phase diagram to give a microvortex phase [20]. Introducing random interactions and/or lack of crystalline order can be a route to obtain spin glass behaviour[138], which has been investigated in for example XY systems with positional disorder[20] or in systems of randomly placed elongated magnets[139]. In addition to constraining the magnetic moments with shape anisotropy, the in-plane magnetization of the nanomagnets can be defined using single crystal materials, restricting the magnetization to point along crystallographic axes. A tuneable dipolar four-state Potts model system can be created employing single crystal nanomagnets with cubic anisotropy, which can order ferromagnetically, antiferromagnetically or in an ice-like manner depending on the relative orientation between the easy axes and bonds connecting the magnets [24] (See **Section 3** and **Figure 3**).

At the boundary between crystals, with perfect discrete translation symmetry, and glasses, with total absence of any such symmetry, lie the quasicrystals. These possess order – by knowing a small part of the structure, one can follow rules to construct the rest of it and fill all of space – but lack discrete translational symmetry. The bulk quasicrystals contain both rare earth [140] and transition metal [141] magnetic species and display spin glass-like freezing when the spins are dilute. For a two-dimensional analogue of a quasicrystal, one can consider the Penrose tiling [142]. Indeed, Heisenberg spins on the nodes of a Penrose tiling have been studied theoretically and recreated as a macroscopic model of magnets [143], and the resulting magnetic configuration can be shown to correspond to interpenetrating non-collinear sublattices in a higher dimensional structure [144]. This work provided the inspiration to build a microscopic artificial analogue of a magnetic quasicrystal placing nanomagnets with Ising-like macrospins along the edges of a Penrose tiling.

Penrose patterns come in two forms, known as kite-and-dart or rhomboid, with the names derived from the shapes of the tiles used to form them. Bhat et al. have constructed Permalloy lattices based on the kite-and-dart form, where the magnetic elements are connected to form a continuous network [145]. These were investigated using the macroscopic probes of SQUID magnetometry and FMR, revealing well-defined switching fields and a rich mode structure. Magnetic imaging of such patterns revealed spatially distinct ordered and frustrated sublattices [17] and reversal by means of two-dimensional avalanches [146], with vortices forming metastable transient states[147]. An artificial magnetic quasicrystal built by placing discrete nanomagnets along the edges of rhomboid tiles (**Figure 6d**) [18], allows the effects of variable coupling to be studied by varying the spacing between the nanomagnets. In contrast to the kite-and-dart quasicrystal, all the links between vertices of the rhomboid tilings are the same length, and this lattice type is less frustrated than the kite-and-dart lattice[148]. With a combination of theoretical considerations and magnetic force microscopy, it was shown that the pattern contains a rigid "skeleton" of moments that spans the patterns and possesses a two-fold degenerate long-range-ordered ground state that surrounds free moments that lead to extensive degeneracy, reminiscent of the heterogeneous ordering in the tetris lattice [15]. This behaviour is similar to the decagonal ordering in a Heisenberg system [143]. In addition to the lack of translational symmetry of the lattice, the quasi-one-dimensional nature of the skeleton enhances the frustration compared to other spin ice systems, such as the square ice. This is because 1D Ising models do not order and means that the ground state is very difficult to access, even by thermal annealing, offering a possible microscopic explanation for the glassy freezing in bulk magnetic quasicrystals.

As many of the examples above illustrate, topologically equivalent geometries can behave very differently due to different point symmetry at the vertices. Lower symmetry at the vertices leads to non-degenerate interactions between the nanomagnets. For example, both the kagome and the brickwork lattice have vertices where three nanomagnets meet but, while the vertices of the kagome lattice gives perfect degeneracy of the vertex states, the vertices in the brickwork lattice are non-degenerate because they are shaped like a 'T'. So even though the pairwise interactions are frustrated in both systems, in the artificial kagome spin ice, any of the three interactions at the vertex can be frustrated, while in the brickwork lattice it is favourable to arrange the frustration on parallel moments. This connection between geometry and frustration limits the way we can design new lattices to study frustration. One can, however, bypass this limitation by going beyond systems where the frustration is a result of pairwise interactions, and rather locate the frustration on the vertices themselves. One way to achieve this is in mixed-coordination systems, where the different vertex types have well-defined low-energy configurations, but they are arranged in such a way that not all vertices can take their lowest energy configuration [149]. Such 'unhappy vertices' thus provide topologically protected excitations above the ground state and, in proper geometries, the degeneracy of the allocation of such vertices grows exponentially with the size of the system leading to a degenerate low-energy manifold [8,150].

6. Conclusions

We highlight here the key directions for future research in the field of artificial spin ice (**Figure 7**). In terms of fundamental science, there are many more geometries and topologies to explore that can lead to the discovery of new emergent phenomena. The exploration of the phase diagrams in artificial spin systems has only recently begun, spurred on by the creation of systems with coupled superparamagnets in thermodynamic equilibrium and the possibilities for characterisation with low energy muon spin spectroscopy,[11] as well as neutron and synchrotron x-ray scattering. In particular, the use of indirect measurement techniques such as resonant soft x-ray scattering [12,97,151,152], neutron scattering and reflectometry [100-102,153], and x-ray photon correlation spectroscopy (XPCS) [82,154] can contribute to further understanding of the long and short-range spatial correlations in these frustrated systems. The low temperature phases in artificial kagome ice have yet to be observed, and there are many different classes of phase transitions to explore, not only Ising but also Kosterlitz-Thouless [22,93,155] and Potts transitions [94] to name a few. For this, not only do the relevant spin-ice geometries need to be created, but characterisation methods need to be developed to measure magnetization dynamics at high spatial and temporal resolution, in order to quantify and classify the transitions unambiguously.

The observation of novel emergent phenomena will be enabled by ever improving nanofabrication methods to create new geometries. Indeed, we have only just started to explore 3D structures, which bring added degrees of freedom [156,157]. One route to create 3D structures is to manufacture layered systems [41,43,158], applying the same lithography methods used to create the 2D systems. Alternatively, 3D structures (see examples in **Figure 5**) can be manufactured with two-photon laser lithography [159-161] to create, for example, a buckyball structure [162], which is a 2D connected spin ice structure wrapped around on itself, and also to manufacture more complex structures [163]. Smaller 3D structures can be made with focused electron beam induced deposition [164,165] and self-assembly methods [153,166,167]. For the creation of novel systems, the only limitation is our imagination and ingenuity to design structures that will generate novel phenomena. In terms of magnetic materials, up to now mainly ferromagnetic thin film materials have been explored, but other materials offer additional functionality to artificial spin ice. For example, in nanomagnets fabricated from ferrimagnetic alloys [87], one can tune the compensation temperature to give specific temperature dependent behaviour of the magnetization, or one can introduce complex anisotropies with single crystal materials [24,168], which can also be adapted by modifying the nanomagnet shape [169]. Interesting behaviour can be obtained with hybrid thin film systems combining, for example, different magnetic thin films, magnetic thin films with superconductors [170,171], or magnetostrictive and piezoelectric materials in so-called multiferroic composites.

In terms of devices, there are many applications where artificial spin ices have the potential to play an important role, including data storage, computation, and encryption, with prospects for their use in the emerging field of unconventional computing, including non-Boolean or neuromorphic computation [172]. For these applications, it will be important to find a way to access the large number of moment configurations [84]. Furthermore, it will be important to develop methods to write data electrically in the form of the magnetic state of individual or collections of magnets utilising, for example, spin orbit torques[173] or spin transfer torques, and to read out the states of individual magnets or an array of magnets with transport measurements [66,99,174]. One might implement magnetic tunnel junctions to access individual nanomagnets, but care would be needed to ensure that the tunnel junctions do not perturb the magnetic configurations in an untoward manner. In addition to electric currents, other stimuli that can be implemented to control the magnetic configurations include electric and magnetic fields[135], strain[58] and heat[57].

The first demonstrations of computation with arrays of magnets exploiting artificial spin ice geometries have been performed [175-178], but there is still quite some way to go in terms of demonstrating functional devices that are CMOS-compatible. Other possibilities for devices include the exploitation of emergent magnetic monopoles, manipulating them in magnetic devices in the same way that the flow of electrons or spins is controlled in electric or spintronic devices.

For this, basic control of monopole propagation has already been demonstrated by modifying the shape of individual nanomagnets (see supplementary information in Ref. [6]). For neuromorphic computing, methods need to be found to mimic the spike-timing-dependent plasticity associated with neurons and eventually to create neural networks. For such bioinspired computation, it will be critical to implement an active or self-regulating control, for example manipulating the magnetic state of individual nanomagnets through strain in a multiferroic composite [58]. It will also be important to be able to tune the interactions between the nanomagnets, something that is just starting to be implemented[48,49,173] and is likely to lead to new phenomena as well as new devices.

Mobile magnetic monopoles are also of interest for high frequency dynamics, in the spirit of previous studies on pyrochlores, where THz and GHz dynamics were used to investigate possibilities for monopole generated responses [179]. The potential to control avalanche dynamics [6] provides a first step towards using artificial spin ice systems as platforms for reprogrammable magnonic resonators and crystals. The flexibility in design may allow, for example, the creation of artificial spin geometries that can channel high frequency excitations along a particular pathway as chosen by the trigger of a specific avalanche or some other mechanism of generating a desired magnetic configuration. Such devices would be of interest as elements in reconfigurable microwave circuits.

Moreover, concepts such as microwave-assisted reversal, which have been pursued for applications in data storage, can inspire new devices constructed from artificial spin ice systems. For example, GHz frequency magnetic fields could be used to guide a frustrated artificial spin ice system into a specific magnetic configuration, which could be exploited in the logic and neuromorphic computing concepts mentioned above. Another route to manipulate magnetic configurations in artificial spin systems is to employ hybrid elements combining nanomagnets with thermoplasmonic heaters, allowing for fast, spatially-selective, and element-specific optical control of local temperatures [180,181].

For devices, both scalability and low power operation are essential. In terms of scalability, it has been shown that artificial spin systems can be fabricated down to the atomic scale with the atoms precisely placed on a surface using a scanning tunnelling microscope tip [182]. While such atomic-scale artificial spin systems can only be realised at low temperatures, the small length scales mean that the interactions can be modified, with the RKKY - like interactions being ferromagnetic or antiferromagnetic depending on the distance between the atoms. These atomic-scale systems may even provide a route to create analogies to the Kitaev model and quantum spin liquids. With a view to low power applications, it would be feasible to create devices working at the Landauer limit [183].

Finally, it should be mentioned that artificial spin systems are not restricted to nanomagnets but can also be implemented with colloids [184-187], superconductors [188,189], and buckled polymer structures [190], and this list is by no means exhaustive. These non-magnetic systems have additional interesting phenomena of their own. For example, in colloidal ice, the ice rule can be destabilised by changing the topology of the lattice by decimation, with effective charges that can rearrange and screen the defects [191]. Artificial spin ice designs can also be used to create systems with a strong plasmonic response [192]. In addition, artificial spin ices made of nanomagnet arrays can be used to control other phenomena including particles for biological applications [193], the behaviour of vortices in superconducting materials [170] or skyrmions[194,195]. The ways in which the field can develop is limited only by the ingenuity of the researchers. Inspiration for the field will continue to increase as the technology evolves to create artificial spin ice geometries at ever decreasing length scales and in three dimensions, to manufacture them from thin film materials with innovative properties and to characterise the spatial correlations at ever faster timescales.

7. Acknowledgements

We are very grateful for the important insights from Peter M. Derlet, Hans-Benjamin Braun, Dirk Grundler, Valerio Scagnoli, Kevin Hofhuis and Quintin N. Meier, which were of great value in the preparation of this manuscript. LH and SHS acknowledge financial support provided by the Swiss National Science Foundation, grant no. 200020_172774.

Box 1 | Emergent magnetic monopoles in artificial spin ice

For the identification of emergent magnetic monopoles in a system consisting of discrete mesoscopic spins, we start with artificial kagome spin ice (top panels) [6,196] and, for simplicity, we create a reference state with all moments pointing to the left by applying a magnetic field to the left (top left panel). We then take the lead from the theoretical description of emergent magnetic monopoles in bulk spin crystals, [25,197] and map each dipole moment to a charge dumbbell (see inset in top left panel). On doing this, we find that the net charge at the vertices will alternate between $Q_0 = +q$ and $Q_0 = -q$, so forming a charge background that is non-zero at the vertices. A string of magnets can then be reversed by applying a magnetic field in the opposite direction. While the vertex charge within the string is the same as the charge background, at one end of the string it exceeds the background vertex charge by $\Delta Q=Q-Q_0=+2q$ (a monopole) and, at the other end, the background charge is reduced by $\Delta Q=Q-Q_0=-2q$ (an antimonopole). This defines emergent magnetic monopoles, i.e. those vertices with $\Delta Q=Q-Q_0=\pm 2q$, as long as there is a dilute population. However, this definition breaks down as magnetization reversal proceeds. One can therefore consider instead a coarse-grained charge density that results from convolution with a Gaussian of width larger than the nearest neighbour distance. The resulting averaged charge density resembles the magnetic flux detected with a magnetic force microscopy (MFM) that cannot distinguish features smaller than the vertex separation. The regions of high and low magnetic flux match very well with the position of the $\Delta Q=\pm 2$ charges, and can now be used to identify the emergent magnetic monopoles at any monopole concentration[6,34]. It is important to note that, as the string expands magnet-by-magnet, the vertex charge, Q, at the ends of the string changes and the emergent magnetic monopoles are not necessarily associated with ice rule breaking vertices. This is an important point; the vertex charge itself is not conserved but the ΔQ charges are topologically protected quasiparticles. Similarly, identifying vertices with $\Delta Q=\pm 2q$ allows us to locate monopoles in the artificial square ice. Here the situation is simpler since the charge background is locally zero so that the change in charge is always equal to the vertex charge ($\Delta Q=Q$). Therefore, not only the emergent magnetic monopoles, but also their respective vertex charges are topologically protected.

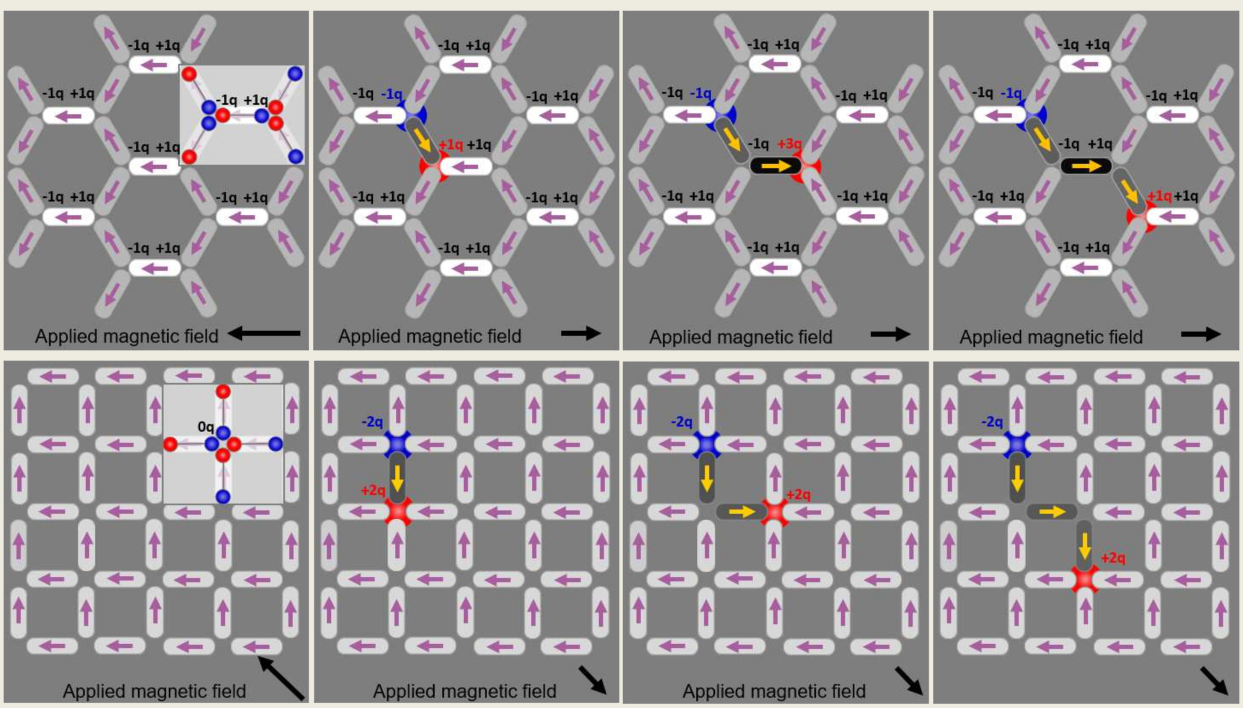

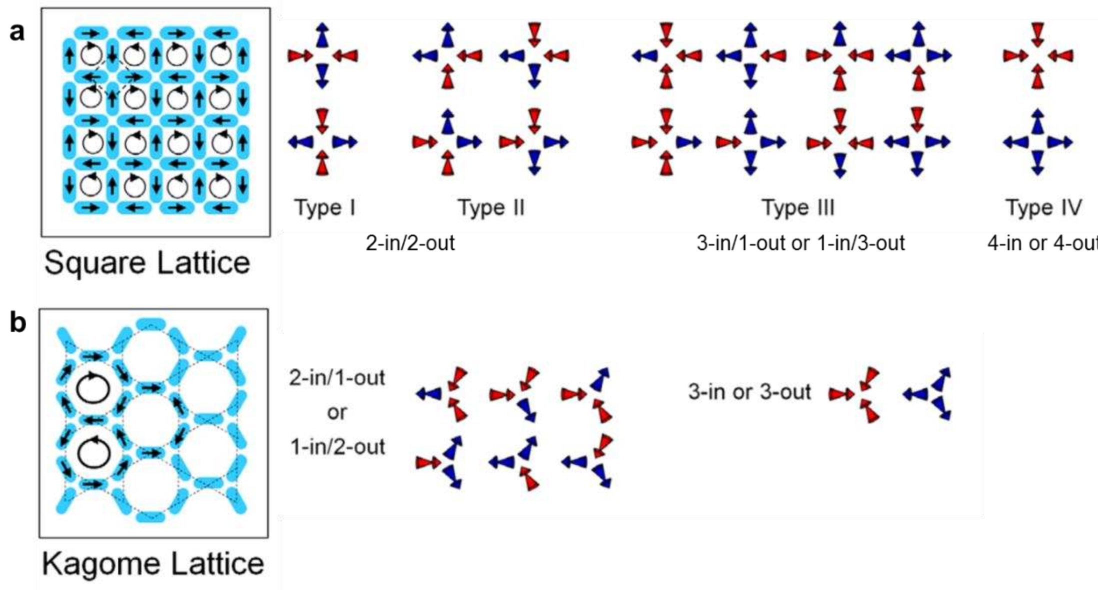

Figure 1 | Classical artificial spin ice systems with elongated single-domain nanomagnets arranged (**a**) on the square lattice and (**b**) on the kagome lattice resulting in a honeycomb structure. To the right, the possible magnetic moment configurations at the vertices are given with the energy of the configurations increasing from left to right.

645

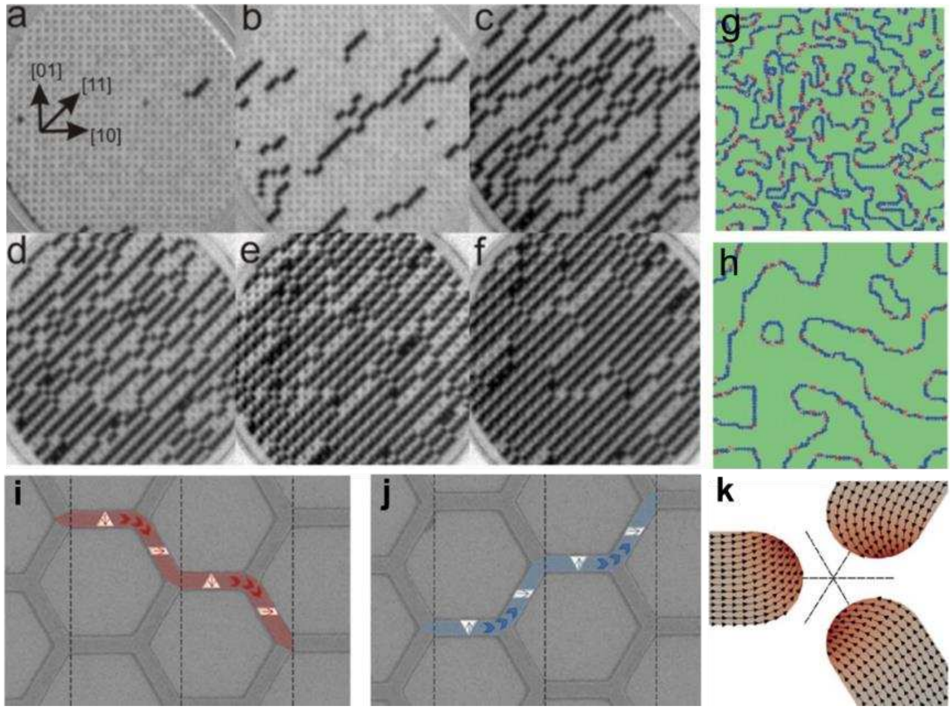

Figure 2 | Propagation and chirality of monopole-like magnetic charges in artificial square ice. a-f | Observation of the creation and separation of charge defects in artificial square ice. Strings of reversed magnets are left behind, which eventually coalesce to form ground state domains separated by domain boundaries [Reprinted from Farhan et al. (supplementary information)[33]]. **g,h |** The domain boundaries themselves contain charge defects, whose motion provides a decrease in the domain wall length and eventually their annihilation (reprinted from Budrikis et al. [39]). **i,j |** Domain walls within the elements of a connected nanowire network have a chirality, with clockwise or anticlockwise rotation of the magnetization within the wall that influences their path through the network (reprinted from Zeissler et al. [60]) **k |** Additional degree of freedom of monopoles arising from the chiral nature of edge bending at a vertex (reprinted from Rougemaille et al. [71]).

646

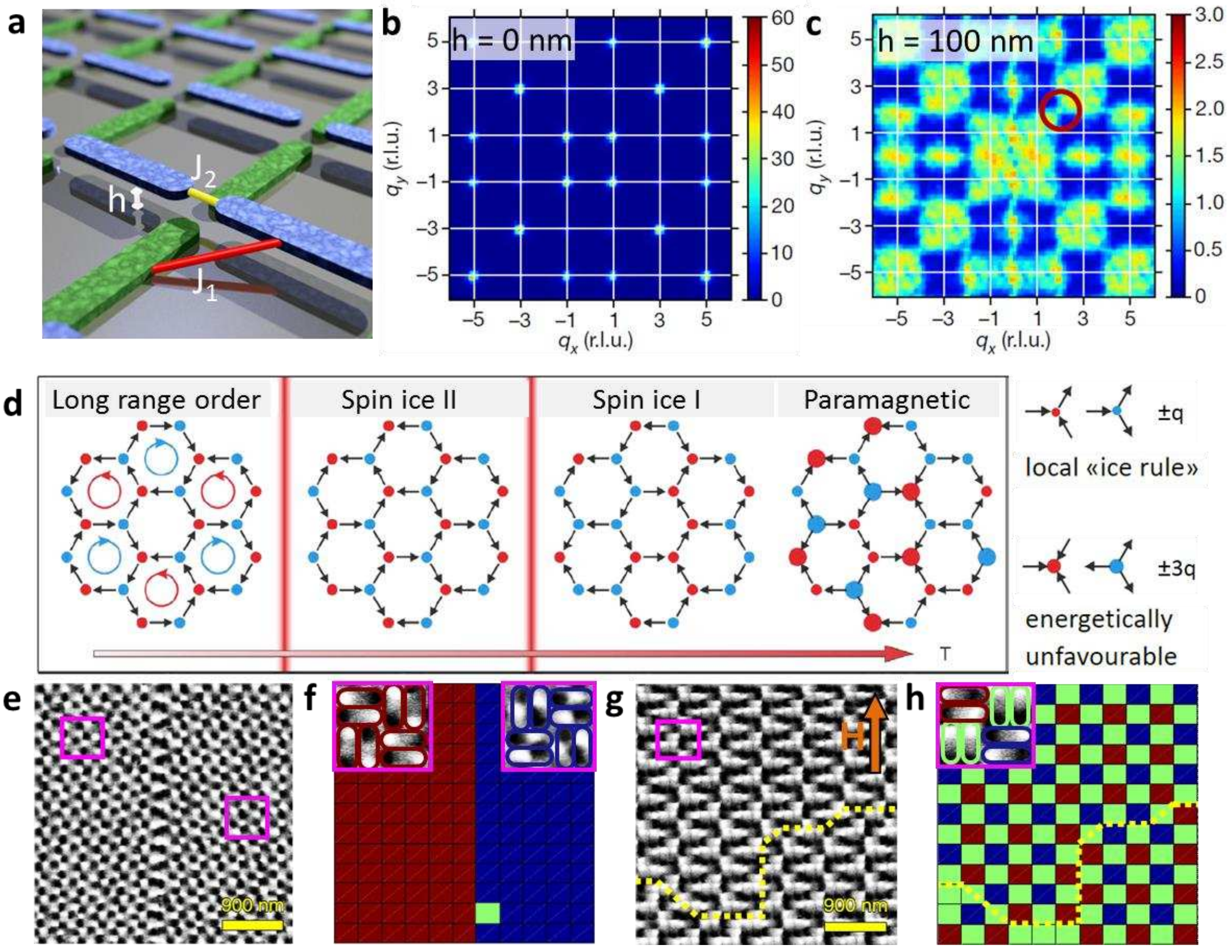

Figure 3 | a | Schematic of an artificial square ice in which one sublattice is offset out of the plane by a height, h, in order to modify the J_1 interactions and **b,c |** magnetic structure factors deduced from MFM images for h=0 nm (**b**) and h=100 nm (**c**). The colour scale refers to the intensity at a given point (q_x, q_y) in reciprocal space. The red circle in **c** encloses a pinch point (Reprinted from Perrin et al. [43]). **d |** Schematics of the predicted magnetic phases as a function of temperature in artificial kagome spin ice. Magnetic charges of opposite sign are indicated in red and blue at the vertices with small dots denoting ±1q and large dots denoting ±3q magnetic charges (Inspired by Möller and Moessner [42]). **e-h |** Ordered Potts states in a 'quadrupolar' ice. Magnetic force microscopy (MFM) image (e) and corresponding bitmap (f) of a zero-field-annealed system favouring a ferro-quadrupolar phase due to strong dipolar interaction between intraplaquette nanomagnet moments. Magnetic force microscopy image (g) and corresponding bitmap (h) of a lattice annealed in a magnetic field favouring an antiferro-quadrupolar phase due to strong dipolar interaction between interplaquette nanomagnet moments. Pink square frames in the MFM images indicate plaquettes of four moment pairs and the colours in the bitmaps represent the different Potts states for the moment pairs, where red and blue denote the ferro-quadrupolar states with opposite chirality (+1 and -1) and green denotes the antiferro-quadrupolar state (Modified from Sklenar et al. [108]).

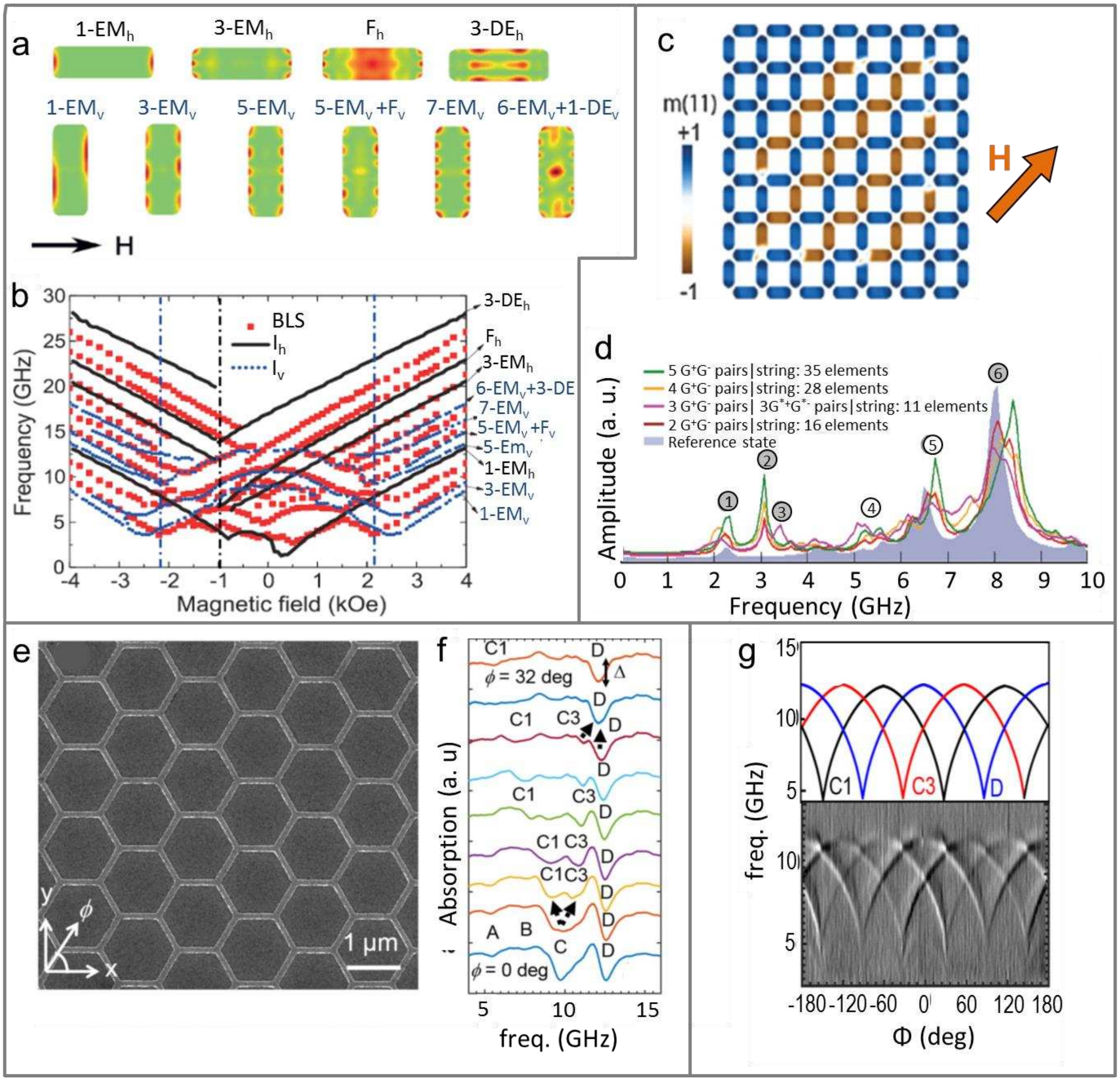

Figure 4 | a,b | Spin wave resonances observed in an artificial square ice using Brillouin light scattering (BLS). Frequencies as a function of magnetic field (**b**) and the corresponding mode profiles (**a**) (reprinted from Li et al. [110]). Red squares are BLS data. Black solid and blue dotted lines are simulation results for horizontal (I_h) and vertical (I_v) isolated islands with respect to the field, respectively. The blue and black dashed dotted vertical lines indicate switching fields of the horizontal and vertical islands, respectively. Labels for the modes indicate eigenmodes with specific spatial characteristics such as an edge mode (EM), a fundamental resonance (F) and a Damon-Eshbach mode (DE). The mode labelled F_h is mainly a standing mode centred in the element with some localisation at the ends. The mode labelled 3-DE_h is a higher order standing mode. The mode shown in the bottom furthest right of panel (a) is a hybrid of two closely spaced modes. **c,d |** Artificial square ice composed of 112 magnetic elements used for simulating spin wave spectra for a magnet field applied in the (11) direction (**c**). The lattice contains four monopole-antimonopole (G^+G^- or $G^{*+}G^{*-}$) pairs connected by Dirac strings extending over 28 elements. (**d**) Spin wave spectra calculated for strings of reversed magnetic elements in an artificial square ice for increasing string length and number of monopole-antimonopole pairs compared to the reference state. The grey shaded number labels correspond to the main, distinct signatures of the topological defects. The resonance peaks shift to larger frequencies when the strings become longer (reprinted from Gliga et al. [52]). **e,f,g |** FMR in a connected artificial kagome spin ice. **e |** SEM image of a connected artificial kagome spin ice. **f |** Resonance response for different directions Φ of the applied magnetic field (H = 1 kOe). At $\Phi=0°$, four modes can be observed, labelled A, B, C and D. The mode C *splits into two modes (C1 and C3) when* Φ *increases, and C3 merges with D at* $\Phi \approx 30°$. The three modes C1, C3 and D originate from elements with the three different orientations. **g |** Spin-wave absorption spectra as a function of in-plane angle Φ *(bottom) combined with a* sketch highlighting the extracted branches (top). The branches corresponding to modes C1, C3 and D are represented by black, red and blue lines, respectively, in the sketch. (Reprinted from Bhat et al. [54]).

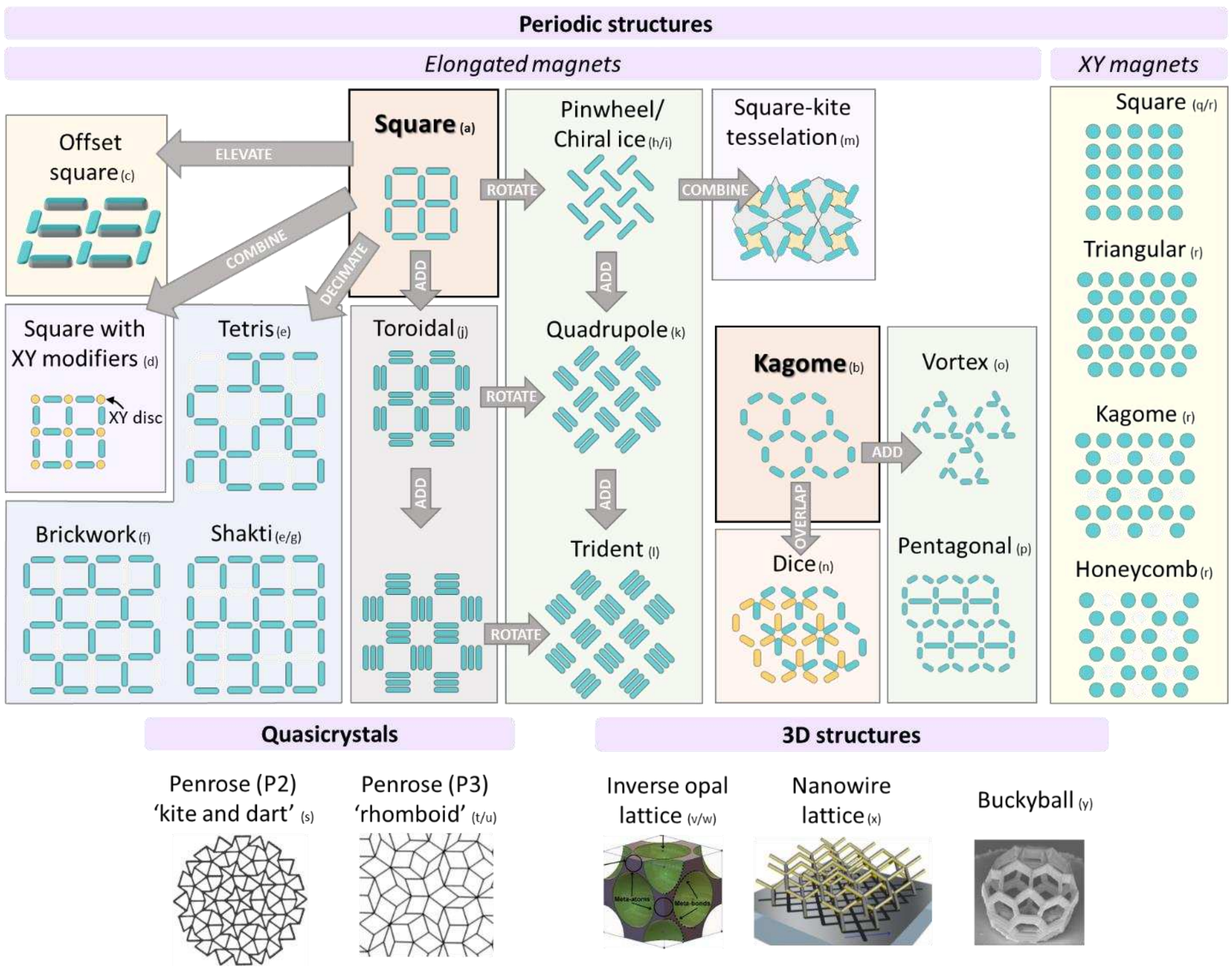

Figure 5 | The family of artificial spin systems going beyond artificial spin ice. Here we highlight some of the connections between the different lattices that have either been realized experimentally or considered theoretically. Other important artificial spin systems omitted from the figure include in-plane magnetization systems with the nanomagnets placed on the Shuriken [198], modified shakti [137], Santa Fe [8], Ising stripe [199] and rectangular [47] lattice. In addition, the in-plane magnetization of the nanomagnets can be further constrained by introducing magnetocrystalline anisotropy, resulting in Potts state magnetic configurations [24]. Another important class of systems that is not shown here consists of magnetic dots with out-of-plane magnetization, which can be fabricated with the same lattice geometries as the XY systems, although their behaviour is fundamentally different [106,200,201]. For the quasicrystal lattices, we highlight connected geometries, although quasicrystal systems made up of individual magnets have also been investigated (See Section 5). In addition to the connected quasicrystal lattices, examples of other lattices with connected elements exist in e.g. square [117], kagome [54] and brickwork [202] geometries. These are topologically equivalent to the antidot lattices [125] mentioned in Section 4 on magnonic crystals and are also interesting networks for the observation of domain wall motion (see Section 2). References a-y are found at the end of the document, before the main reference list.

References for Figure 5:

a) Wang, R. F. et al. Artificial ‘spin ice’ in a geometrically frustrated lattice of nanoscale ferromagnetic islands. Nature **439**, 303–306 (2006).[1]
b) Möller, G. & Moessner, R. Artificial Square Ice and Related Dipolar Nanoarrays. Phys. Rev. Lett. **96**, 237202 (2006).[42]
c) Perrin, Y., Canals, B. & Rougemaille, N. Extensive degeneracy, Coulomb phase and magnetic monopoles in artificial square ice. Nature **540**, 410 (2016).[43]
d) Östman, E. et al. Interaction modifiers in artificial spin ices. Nat. Phys. **14**, 375-379 (2018).[21]
e) Gilbert, I. et al. Emergent reduced dimensionality by vertex frustration in artificial spin ice. Nat. Phys. **12**, 162 (2016).[15]
f) Park, J. et al. Magnetic response of brickwork artificial spin ice. Phys. Rev. B **96**, 024436 (2017).[202]
g) Lao, Y. et al. Classical topological order in the kinetics of artificial spin ice. Nat. Phys. **14**, 723-727 (2018).[14]
h) Gliga, S. et al. Emergent dynamic chirality in a thermally driven artificial spin ratchet. Nat. Mater. **16**, 1106 (2017).[9]
i) Macêdo, R., Macauley, G. M., Nascimento, F. S. & Stamps, R. L. Apparent ferromagnetism in the pinwheel artificial spin ice. Phys. Rev. B **98**, 014437 (2018).[131]
j) Lehmann, J., Donnelly, C., Derlet, P. M., Heyderman, L. J. & Fiebig, M. Poling of an artificial magneto-toroidal crystal. Nat. Nanotechnol. **14**, 141-144 (2018).[134]
k) Sklenar, J. et al. Field-induced phase coexistence in an artificial spin ice. Nat. Phys. **15**, 191-195 (2018). [108]
l) Farhan, A. et al. Nanoscale control of competing interactions and geometrical frustration in a dipolar trident lattice. Nat. Commun. **8**, 995 (2017).[130]
m) Petersen, C. F. et al. Tuning magnetic ordering in a dipolar square-kite tessellation. Appl. Phys. Lett. **112**, 092403 (2018).[105]
n) Farhan, A. et al. Thermodynamics of emergent magnetic charge screening in artificial spin ice. Nat. Commun. **7**, 12635 (2016).[16]
o) Yu, L. et al. Monte Carlo simulation on a new artificial spin ice lattice consisting of hexagons and three-moment vertices. AIP Advances **7**, 085211 (2017).[133]
p) Chern, G.-W. & Mellado, P. Magnetic monopole polarons in artificial spin ices. EPL **114**, 37004 (2016).[55]
q) Leo, N. et al. Collective magnetism in an artificial 2D XY spin system. Nat. Commun. **9**, 2850 (2018).[19]
r) Streubel, R. et al. Spatial and Temporal Correlations of XY Macro Spins. Nano Lett. **18**, 7428-7434 (2018). [22]
s) Farmer, B. et al. Direct imaging of coexisting ordered and frustrated sublattices in artificial ferromagnetic quasicrystals. Phys. Rev. B **93**, 134428 (2016).[17]
t) Shi, D. et al. Frustration and thermalization in an artificial magnetic quasicrystal. Nat. Phys. **14**, 309–314 (2018). [18]
u) Vedmedenko, E. Y., Oepen, H. P. & Kirschner, J. Decagonal Quasiferromagnetic Microstructure on the Penrose Tiling. Phys. Rev. Lett. **90**, 137203 (2003).[143]
v) Liu, Y. et al. Confined Chemical Fluid Deposition of Ferromagnetic Metalattices. Nano Lett. **18**, 546–552 (2018).[203]
w) Mistonov, A. A. et al. Magnetic structure of the inverse opal-like structures: small angle neutron diffraction and micromagnetic simulations. J. Magn. Magn. Mater. **477**, 99-108 (2019). [153]
x) May, A., Hunt, M., Berg, A. V. D., Hejazi, A. & Ladak, S. Realisation of a frustrated 3D magnetic nanowire lattice. Commun. Phys. **2**, 13 (2019).[161]
y) Donnelly, C. et al. Element-Specific X-Ray Phase Tomography of 3D Structures at the Nanoscale. Phys. Rev. Lett. **114**, 115501 (2015).[162]

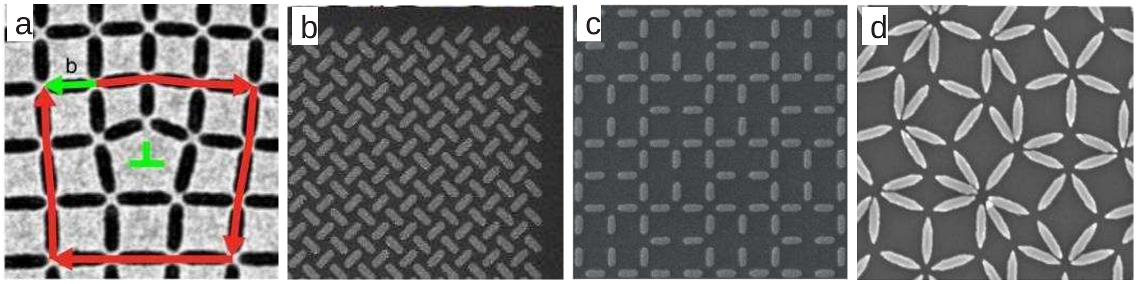

Figure 6 | Experimental realisations of selected artificial spin ice geometries. **a |** In-focus transmission electron micrograph of a dislocation point defect in an artificial square ice. The Burgers circuit and vector **b** are shown in red and green, respectively (reprinted from Drisko et al. [37]). **b |** Scanning electron micrograph of part of a chiral ice array, based on rotating every element of a square ice through an angle of 45°. This results in a dynamic chirality with the magnetization rotating in one sense during thermal relaxation (reprinted from Gliga et al. [9]). **c |** Scanning electron micrograph of part of a shakti lattice (reprinted from Gilbert et al. [7]). **d |** Scanning electron micrograph of part of a rhomboid quasiperiodic Penrose tiling similar to that studied by Shi et al. [18].

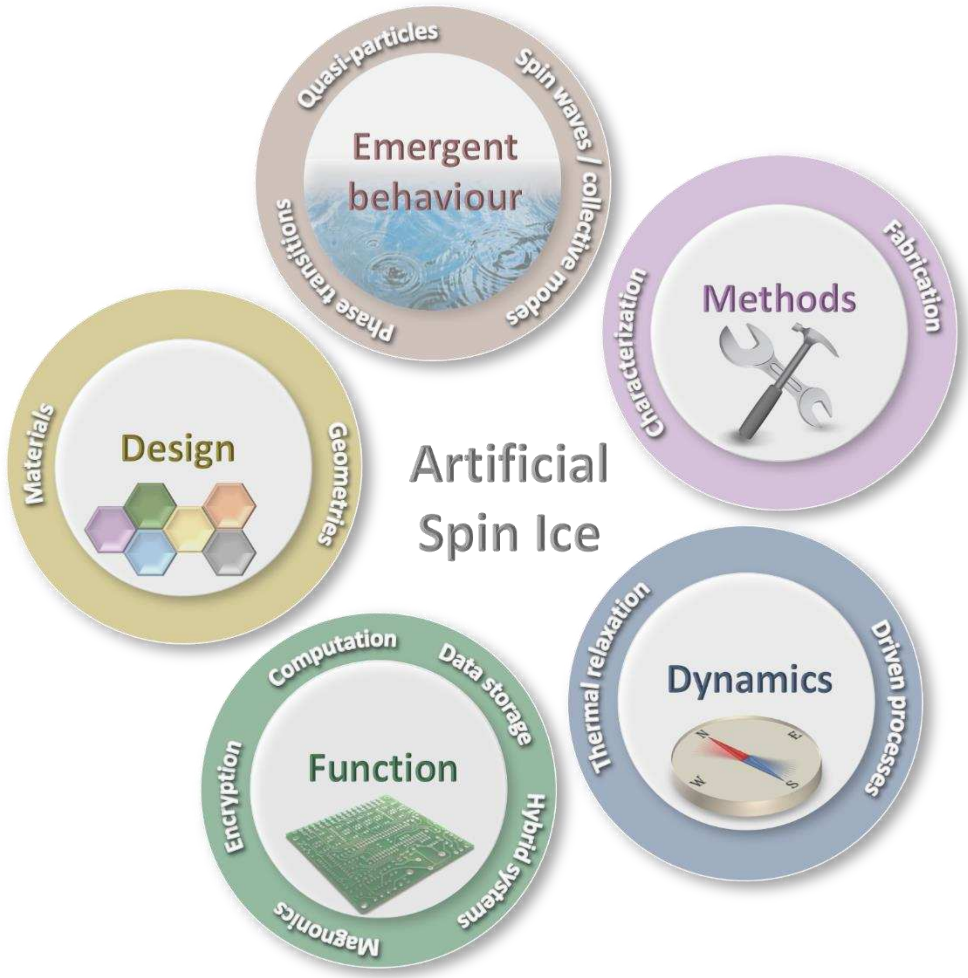

Figure 7 | Key directions for future research in artificial spin ice.

702

Bibliography

1 Wang, R. F. *et al.* Artificial 'spin ice' in a geometrically frustrated lattice of nanoscale ferromagnetic islands. *Nature* **439**, 303-306, doi:10.1038/nature04447 (2006).

2 Harris, M. J., Bramwell, S. T., McMorrow, D. F., Zeiske, T. & Godfrey, K. W. Geometrical Frustration in the Ferromagnetic Pyrochlore $Ho_2Ti_2O_7$. *Phys. Rev. Lett.* **79**, 2554-2557, doi:10.1103/PhysRevLett.79.2554 (1997).

3 Heyderman, L. J. & Stamps, R. L. Artificial ferroic systems: novel functionality from structure, interactions and dynamics. *J. Phys.: Condens. Matter* **25**, 363201, doi:10.1088/0953-8984/25/36/363201 (2013).

4 Nisoli, C., Moessner, R. & Schiffer, P. Colloquium: Artificial spin ice: Designing and imaging magnetic frustration. *Rev. Mod. Phys.* **85**, 1473-1490, doi:10.1103/RevModPhys.85.1473 (2013).

5 Ladak, S., Read, D. E., Perkins, G. K., Cohen, L. F. & Branford, W. R. Direct observation of magnetic monopole defects in an artificial spin-ice system. *Nat. Phys.* **6**, 359-363, doi:10.1038/nphys1628 (2010).

6 Mengotti, E. *et al.* Real-space observation of emergent magnetic monopoles and associated Dirac strings in artificial kagome spin ice. *Nat. Phys.* **7**, 68, doi:10.1038/nphys1794 (2011).

7 Gilbert, I. *et al.* Emergent ice rule and magnetic charge screening from vertex frustration in artificial spin ice. *Nat. Phys.* **10**, 670-675, doi:10.1038/nphys3037 (2014).

8 Morrison, M. J., Nelson, T. R. & Nisoli, C. Unhappy vertices in artificial spin ice: new degeneracies from vertex frustration. *New J. Phys.* **15**, 045009, doi:10.1088/1367-2630/15/4/045009 (2013).

9 Gliga, S. *et al.* Emergent dynamic chirality in a thermally driven artificial spin ratchet. *Nat. Mater.* **16**, 1106, doi:10.1038/nmat5007 (2017).

10 Kapaklis, V. *et al.* Melting artificial spin ice. *New J. Phys.* **14**, 035009, doi:10.1088/1367-2630/14/3/035009 (2012).

11 Anghinolfi, L. *et al.* Thermodynamic phase transitions in a frustrated magnetic metamaterial. *Nat. Commun.* **6**, 8278, doi:10.1038/ncomms9278 (2015).

12 Sendetskyi, O. *et al.* Continuous magnetic phase transition in artificial square ice. *Phys. Rev. B* **99**, 214430, doi:10.1103/PhysRevB.99.214430 (2019).

13 Krawczyk, M. & Grundler, D. Review and prospects of magnonic crystals and devices with reprogrammable band structure. *J. Phys.: Condens. Matter* **26**, 123202, doi:10.1088/0953-8984/26/12/123202 (2014).

14 Lao, Y. *et al.* Classical topological order in the kinetics of artificial spin ice. *Nat. Phys.* **14**, 723-727, doi:10.1038/s41567-018-0077-0 (2018).

15 Gilbert, I. *et al.* Emergent reduced dimensionality by vertex frustration in artificial spin ice. *Nat. Phys.* **12**, 162, doi:10.1038/nphys3520 (2016).

16 Farhan, A. *et al.* Thermodynamics of emergent magnetic charge screening in artificial spin ice. *Nat. Commun.* **7**, 12635, doi:10.1038/ncomms12635 (2016).

17 Farmer, B. *et al.* Direct imaging of coexisting ordered and frustrated sublattices in artificial ferromagnetic quasicrystals. *Phys. Rev. B* **93**, 134428, doi:10.1103/PhysRevB.93.134428 (2016).

18 Shi, D. *et al.* Frustration and thermalization in an artificial magnetic quasicrystal. *Nat. Phys.* **14**, 309-314, doi:10.1038/s41567-017-0009-4 (2018).

19 Leo, N. *et al.* Collective magnetism in an artificial 2D XY spin system. *Nat. Commun.* **9**, 2850, doi:10.1038/s41467-018-05216-2 (2018).

20 Schildknecht, D., Heyderman, L. J. & Derlet, P. M. Phase diagram of dipolar-coupled XY moments on disordered square lattices. *Phys. Rev. B* **98**, 064420, doi:10.1103/PhysRevB.98.064420 (2018).

21 Östman, E. *et al.* Interaction modifiers in artificial spin ices. *Nat. Phys.* **14**, 375-379, doi:10.1038/s41567-017-0027-2 (2018).

22 Streubel, R. *et al.* Spatial and Temporal Correlations of XY Macro Spins. *Nano Lett.* **18**, 7428-7434, doi:10.1021/acs.nanolett.8b01789 (2018).

23 Velten, S. *et al.* Vortex circulation patterns in planar microdisk arrays. *Appl. Phys. Lett.* **110**, 262406, doi:10.1063/1.4990990 (2017).

24 Louis, D. *et al.* A tunable magnetic metamaterial based on the dipolar four-state Potts model. *Nat. Mater.* **17**, 1076, doi:10.1038/s41563-018-0199-x (2018).

25 Castelnovo, C., Moessner, R. & Sondhi, S. L. Magnetic monopoles in spin ice. *Nature* **451**, 42-45, doi:10.1038/nature06433 (2008).

26 Fennell, T. *et al.* Magnetic Coulomb Phase in the Spin Ice $Ho_2Ti_2O_7$. *Science* **326**, 415-417, doi:10.1126/science.1177582 (2009).

27 Kadowaki, H. *et al.* Observation of Magnetic Monopoles in Spin Ice. *J. Phys. Soc. Jpn.* **78**, 103706, doi:10.1143/JPSJ.78.103706 (2009).

28 Morris, D. J. P. *et al.* Dirac Strings and Magnetic Monopoles in the Spin Ice $Dy_2Ti_2O_7$. *Science* **326**, 411-414, doi:10.1126/science.1178868 (2009).

29 Bramwell, S. T. *et al.* Measurement of the charge and current of magnetic monopoles in spin ice. *Nature* **461**, 956-959, doi:10.1038/nature08500 (2009).

30 Mól, L. A. *et al.* Magnetic monopole and string excitations in two-dimensional spin ice. *J. Appl. Phys.* **106**, 063913, doi:10.1063/1.3224870 (2009).

31 León, A. Heavy and light monopoles in magnetic reversion in artificial spin ice. *Curr. Appl. Phys.* **13**, 2014-2018, doi:10.1016/j.cap.2013.08.010 (2013).

32 Gilbert, I. *et al.* Direct visualization of memory effects in artificial spin ice. *Phys. Rev. B* **92**, 104417, doi:10.1103/PhysRevB.92.104417 (2015).

33 Farhan, A. *et al.* Direct Observation of Thermal Relaxation in Artificial Spin Ice. *Phys. Rev. Lett.* **111**, 057204, doi:10.1103/PhysRevLett.111.057204 (2013).

34 Farhan, A., Derlet, P. M., Anghinolfi, L., Kleibert, A. & Heyderman, L. J. Magnetic charge and moment dynamics in artificial kagome spin ice. *Phys. Rev. B* **96**, 064409, doi:10.1103/PhysRevB.96.064409 (2017).

35 Silva, R. C. *et al.* Nambu monopoles interacting with lattice defects in a two-dimensional artificial square spin ice. *Phys. Rev. B* **87**, 014414, doi:10.1103/PhysRevB.87.014414 (2013).

36 Thonig, D. & Henk, J. Pinning of thermal excitations at defects in artificial dipolar arrays: A theoretical investigation. *J. Magn. Magn. Mater.* **386**, 117-124, doi:10.1016/j.jmmm.2015.03.048 (2015).

37 Drisko, J., Marsh, T. & Cumings, J. Topological frustration of artificial spin ice. *Nat. Commun.* **8**, ncomms14009, doi:10.1038/ncomms14009 (2017).

38 Vedmedenko, E. Y. Dynamics of Bound Monopoles in Artificial Spin Ice: How to Store Energy in Dirac Strings. *Phys. Rev. Lett.* **116**, 077202, doi:10.1103/PhysRevLett.116.077202 (2016).

39 Budrikis, Z. *et al.* Domain dynamics and fluctuations in artificial square ice at finite temperatures. *New J. Phys.* **14**, 035014, doi:10.1088/1367-2630/14/3/035014 (2012).

40 Mól, L. A. S., Moura-Melo, W. A. & Pereira, A. R. Conditions for free magnetic monopoles in nanoscale square arrays of dipolar spin ice. *Phys. Rev. B* **82**, 054434, doi:10.1103/PhysRevB.82.054434 (2010).

41 Chern, G.-W., Reichhardt, C. & Nisoli, C. Realizing three-dimensional artificial spin ice by stacking planar nano-arrays. *Appl. Phys. Lett.* **104**, 013101, doi:10.1063/1.4861118 (2014).

42 Möller, G. & Moessner, R. Artificial Square Ice and Related Dipolar Nanoarrays. *Phys. Rev. Lett.* **96**, 237202, doi:10.1103/PhysRevLett.96.237202 (2006).

43 Perrin, Y., Canals, B. & Rougemaille, N. Extensive degeneracy, Coulomb phase and magnetic monopoles in artificial square ice. *Nature* **540**, 410, doi:10.1038/nature20155 (2016).

44 Farhan, A. *et al.* Emergent magnetic monopole dynamics in macroscopically degenerate artificial spin ice. *Sci. Adv.* **5**, eaav6380, doi:10.1126/sciadv.aav6380 (2019).

45 Henley, C. L. The "Coulomb Phase" in Frustrated Systems. *Annu. Rev. Condens. Matter Phys.* **1**, 179-210, doi:10.1146/annurev-conmatphys-070909-104138 (2010).

46 Ribeiro, I. R. B. *et al.* Realization of Rectangular Artificial Spin Ice and Direct Observation of High Energy Topology. *Sci. Rep.* **7**, 13982, doi:10.1038/s41598-017-14421-w (2017).

47 Loreto, R. P. *et al.* Experimental and theoretical evidences for the ice regime in planar artificial spin ices. *J. Phys.: Condens. Matter* **31**, 025301, doi:10.1088/1361-648X/aaeeef (2019).

48 Perrin, Y., Canals, B. & Rougemaille, N. Quasidegenerate ice manifold in a purely two-dimensional square array of nanomagnets. *Phys. Rev. B* **99**, 224434, doi:10.1103/PhysRevB.99.224434 (2019).

49 Schanilec, V., Perrin, Y., Denmat, S. L., Canals, B. & Rougemaille, N. Artificial vertex systems by design. *arXiv:1902.00452 [cond-mat]* (2019).

50 Takatsu, H. *et al.* Two-Dimensional Monopole Dynamics in the Dipolar Spin Ice $Dy_2Ti_2O_7$. *J. Phys. Soc. Jpn.* **82**, 073707, doi:10.7566/JPSJ.82.073707 (2013).

51 Otsuka, H., Takatsu, H., Goto, K. & Kadowaki, H. Scaling ansatz for the ac magnetic response in two-dimensional spin ice. *Phys. Rev. B* **90**, 144428, doi:10.1103/PhysRevB.90.144428 (2014).

52 Gliga, S., Kákay, A., Hertel, R. & Heinonen, O. G. Spectral Analysis of Topological Defects in an Artificial Spin-Ice Lattice. *Phys. Rev. Lett.* **110**, 117205, doi:10.1103/PhysRevLett.110.117205 (2013).

53 Bhat, V. S., Heimbach, F., Stasinopoulos, I. & Grundler, D. Magnetization dynamics of topological defects and the spin solid in a kagome artificial spin ice. *Phys. Rev. B* **93**, 140401, doi:10.1103/PhysRevB.93.140401 (2016).

54 Bhat, V. S., Heimbach, F., Stasinopoulos, I. & Grundler, D. Angular-dependent magnetization dynamics of kagome artificial spin ice incorporating topological defects. *Phys. Rev. B* **96**, 014426, doi:10.1103/PhysRevB.96.014426 (2017).

55 Chern, G.-W. & Mellado, P. Magnetic monopole polarons in artificial spin ices. *EPL* **114**, 37004, doi:10.1209/0295-5075/114/37004 (2016).

56 Loreto, R. P. *et al.* Emergence and mobility of monopoles in a unidirectional arrangement of magnetic nanoislands. *Nanotechnology* **26**, 295303, doi:10.1088/0957-4484/26/29/295303 (2015).

57 León, A. Thermal phase transition in artificial spin ice systems induces the formation and migration of monopole-like magnetic excitations. *Physica B* **500**, 59-65, doi:10.1016/j.physb.2016.07.012 (2016).

58 Chavez, A. C., Barra, A. & Carman, G. P. Voltage control of magnetic monopoles in artificial spin ice. *J. Phys. D: Appl. Phys.* **51**, 234001, doi:10.1088/1361-6463/aac0ae (2018).

59 Mellado, P., Petrova, O., Shen, Y. & Tchernyshyov, O. Dynamics of Magnetic Charges in Artificial Spin Ice. *Phys. Rev. Lett.* **105**, 187206, doi:10.1103/PhysRevLett.105.187206 (2010).

60 Zeissler, K. *et al.* The non-random walk of chiral magnetic charge carriers in artificial spin ice. *Sci. Rep.* **3**, 1252, doi:10.1038/srep01252 (2013).

61 Pushp, A. *et al.* Domain wall trajectory determined by its fractional topological edge defects. *Nat. Phys.* **9**, 505-511, doi:10.1038/nphys2669 (2013).

62 Omari, K. A. & Hayward, T. J. Chirality-Based Vortex Domain-Wall Logic Gates. *Phys. Rev. Applied* **2**, 044001, doi:10.1103/PhysRevApplied.2.044001 (2014).

63 Garg, C. *et al.* Highly Asymmetric Chiral Domain-Wall Velocities in Y-Shaped Junctions. *Nano Lett.* **18**, 1826-1830, doi:10.1021/acs.nanolett.7b05086 (2018).

64 Burn, D. M., Chadha, M., Walton, S. K. & Branford, W. R. Dynamic interaction between domain walls and nanowire vertices. *Phys. Rev. B* **90**, 144414, doi:10.1103/PhysRevB.90.144414 (2014).

65 Walton, S. K. *et al.* Limitations in artificial spin ice path selectivity: the challenges beyond topological control. *New J. Phys.* **17**, 013054, doi:10.1088/1367-2630/17/1/013054 (2015).

66 Burn, D. M., Chadha, M. & Branford, W. R. Dynamic dependence to domain wall propagation through artificial spin ice. *Phys. Rev. B* **95**, 104417, doi:10.1103/PhysRevB.95.104417 (2017).

67 Burn, D. M., Chadha, M. & Branford, W. R. Angular-dependent magnetization reversal processes in artificial spin ice. *Phys. Rev. B* **92**, 214425, doi:10.1103/PhysRevB.92.214425 (2015).

68 Kwon, J. *et al.* Low field domain wall dynamics in artificial spin-ice basis structure. *J. Appl. Phys.* **118**, 163907, doi:10.1063/1.4934733 (2015).

69 Sethi, P. *et al.* Direct observation of deterministic domain wall trajectory in magnetic network structures. *Sci. Rep.* **6**, doi:10.1038/srep19027 (2016).

70 Gartside, J. C. *et al.* Realization of ground state in artificial kagome spin ice via topological defect-driven magnetic writing. *Nat. Nanotechnol.* **13**, 53, doi:10.1038/s41565-017-0002-1 (2018).

71 Rougemaille, N. *et al.* Chiral nature of magnetic monopoles in artificial spin ice. *New J. Phys.* **15**, 035026, doi:10.1088/1367-2630/15/3/035026 (2013).

72 Nisoli, C. *et al.* Effective temperature in an interacting vertex system: theory and experiment on artificial spin ice. *Phys. Rev. Lett.* **105**, 047205, doi:10.1103/PhysRevLett.105.047205 (2010).

73 Morgan, J. P. *et al.* Real and effective thermal equilibrium in artificial square spin ices. *Phys. Rev. B* **87**, 024405, doi:10.1103/PhysRevB.87.024405 (2013).

74 Lammert, P. E. *et al.* Direct entropy determination and application to artificial spin ice. *Nat. Phys.* **6**, 786-789, doi:10.1038/nphys1728 (2010).

75 Porro, J. M., Bedoya-Pinto, A., Berger, A. & Vavassori, P. Exploring thermally induced states in square artificial spin-ice arrays. *New J. Phys.* **15**, 055012, doi:10.1088/1367-2630/15/5/055012 (2013).

76 Zhang, S. *et al.* Crystallites of magnetic charges in artificial spin ice. *Nature* **500**, 553-557, doi:10.1038/nature12399 (2013).

77 Drisko, J., Daunheimer, S. & Cumings, J. $FePd_3$ as a material for studying thermally active artificial spin ice systems. *Phys. Rev. B* **91**, 224406, doi:10.1103/PhysRevB.91.224406 (2015).

78 Ke, X. *et al.* Energy Minimization and ac Demagnetization in a Nanomagnet Array. *Phys. Rev. Lett.* **101**, 037205, doi:10.1103/PhysRevLett.101.037205 (2008).

79 Budrikis, Z. *et al.* Disorder Strength and Field-Driven Ground State Domain Formation in Artificial Spin Ice: Experiment, Simulation, and Theory. *Phys. Rev. Lett.* **109**, 037203, doi:10.1103/PhysRevLett.109.037203 (2012).

80 Coey, J. M. D. *Magnetism and Magnetic Materials*. (Cambridge University Press, 2010).

81 Osborn, J. A. Demagnetizing Factors of the General Ellipsoid. *Phys. Rev.* **67**, 351-357, doi:10.1103/PhysRev.67.351 (1945).

82 Morley, S. A. *et al.* Vogel-Fulcher-Tammann freezing of a thermally fluctuating artificial spin ice probed by x-ray photon correlation spectroscopy. *Phys. Rev. B* **95**, 104422, doi:10.1103/PhysRevB.95.104422 (2017).

83 Andersson, M. S. *et al.* Thermally induced magnetic relaxation in square artificial spin ice. *Sci. Rep.* **6**, 37097, doi:10.1038/srep37097 (2016).

84 Farhan, A. *et al.* Exploring hyper-cubic energy landscapes in thermally active finite artificial spin-ice systems. *Nat. Phys.* **9**, 375-382, doi:10.1038/nphys2613 (2013).

85 Kapaklis, V. *et al.* Thermal fluctuations in artificial spin ice. *Nat. Nanotechnol.* **9**, 514-519, doi:10.1038/nnano.2014.104 (2014).

86 Morley, S. A. *et al.* Effect of FePd alloy composition on the dynamics of artificial spin ice. *Sci. Rep.* **8**, 4750, doi:10.1038/s41598-018-23208-6 (2018).

87 Montaigne, F. *et al.* Size distribution of magnetic charge domains in thermally activated but out-of-equilibrium artificial spin ice. *Sci. Rep.* **4**, 5702, doi:10.1038/srep05702 (2014).

88 Rougemaille, N. & Canals, B. Cooperative magnetic phenomena in artificial spin systems: spin liquids, Coulomb phase and fragmentation of magnetism – a colloquium. *Eur. Phys. J. B* **92**, 62, doi:10.1140/epjb/e2018-90346-7 (2019).

89 Morgan, J. P., Stein, A., Langridge, S. & Marrows, C. H. Thermal ground-state ordering and elementary excitations in artificial magnetic square ice. *Nat. Phys.* **7**, 75, doi:10.1038/nphys1853 (2011).

90 Silva, R. C., Nascimento, F. S., Mól, L. A. S., Moura-Melo, W. A. & Pereira, A. R. Thermodynamics of elementary excitations in artificial magnetic square ice. *New J. Phys.* **14**, 015008, doi:10.1088/1367-2630/14/1/015008 (2012).

91 Levis, D., Cugliandolo, L. F., Foini, L. & Tarzia, M. Thermal Phase Transitions in Artificial Spin Ice. *Phys. Rev. Lett.* **110**, 207206, doi:10.1103/PhysRevLett.110.207206 (2013).

92 Parakkat, V. M., Xie, K. & Krishnan, K. M. Tunable ground state in heterostructured artificial spin ice with exchange bias. *Phys. Rev. B* **99**, 054429, doi:10.1103/PhysRevB.99.054429 (2019).

93 Chern, G.-W., Mellado, P. & Tchernyshyov, O. Two-Stage Ordering of Spins in Dipolar Spin Ice on the Kagome Lattice. *Phys. Rev. Lett.* **106**, 207202, doi:10.1103/PhysRevLett.106.207202 (2011).

94 Chern, G.-W. & Tchernyshyov, O. Magnetic charge and ordering in kagome spin ice. *Phil. Trans. R. Soc. A* **370**, 5718-5737, doi:10.1098/rsta.2011.0388 (2012).

95 Canals, B. *et al.* Fragmentation of magnetism in artificial kagome dipolar spin ice. *Nat. Commun.* **7**, 11446, doi:10.1038/ncomms11446 (2016).

96 Brooks-Bartlett, M. E., Banks, S. T., Jaubert, L. D. C., Harman-Clarke, A. & Holdsworth, P. C. W. Magnetic-Moment Fragmentation and Monopole Crystallization. *Phys. Rev. X* **4**, 011007, doi:10.1103/PhysRevX.4.011007 (2014).

97 Sendetskyi, O. *et al.* Magnetic diffuse scattering in artificial kagome spin ice. *Phys. Rev. B* **93**, 224413, doi:10.1103/PhysRevB.93.224413 (2016).

98 Farhan, A. *et al.* Thermally induced magnetic relaxation in building blocks of artificial kagome spin ice. *Phys. Rev. B* **89**, 214405, doi:10.1103/PhysRevB.89.214405 (2014).

99 Branford, W. R., Ladak, S., Read, D. E., Zeissler, K. & Cohen, L. F. Emerging Chirality in Artificial Spin Ice. *Science* **335**, 1597-1600, doi:10.1126/science.1211379 (2012).

100 Summers, B., Chen, Y., Dahal, A. & Singh, D. K. New Description of Evolution of Magnetic Phases in Artificial Honeycomb Lattice. *Sci. Rep.* **7**, 16080, doi:10.1038/s41598-017-15786-8 (2017).

101 Glavic, A. *et al.* Spin Solid versus Magnetic Charge Ordered State in Artificial Honeycomb Lattice of Connected Elements. *Adv. Sci.*, 1700856, doi:10.1002/advs.201700856 (2018).

102 Summers, B. *et al.* Temperature-dependent magnetism in artificial honeycomb lattice of connected elements. *Phys. Rev. B* **97**, 014401, doi:10.1103/PhysRevB.97.014401 (2018).

103 Chioar, I. A. *et al.* Kinetic pathways to the magnetic charge crystal in artificial dipolar spin ice. *Phys. Rev. B* **90**, 220407, doi:10.1103/PhysRevB.90.220407 (2014).

104 Liashko, S. Y., Jónsson, H. & Uzdin, V. M. The effect of temperature and external field on transitions in elements of kagome spin ice. *New J. Phys.* **19**, 113008, doi:10.1088/1367-2630/aa8b96 (2017).

105 Petersen, C. F. *et al.* Tuning magnetic ordering in a dipolar square-kite tessellation. *Appl. Phys. Lett.* **112**, 092403, doi:10.1063/1.5014041 (2018).

106 Chioar, I. A. *et al.* Nonuniversality of artificial frustrated spin systems. *Phys. Rev. B* **90**, 064411, doi:10.1103/PhysRevB.90.064411 (2014).

107 Hamp, J., Moessner, R. & Castelnovo, C. Supercooling and fragile glassiness in a dipolar kagome Ising magnet. *Phys. Rev. B* **98**, 144439, doi:10.1103/PhysRevB.98.144439 (2018).

108 Sklenar, J. *et al.* Field-induced phase coexistence in an artificial spin ice. *Nat. Phys.* **15**, 191-195, doi:10.1038/s41567-018-0348-9 (2018).

109 Carlotti, G. *et al.* From micro- to nanomagnetic dots: evolution of the eigenmode spectrum on reducing the lateral size. *J. Phys. D: Appl. Phys.* **47**, 265001, doi:10.1088/0022-3727/47/26/265001 (2014).

110 Li, Y. *et al.* Thickness dependence of spin wave excitations in an artificial square spin ice-like geometry. *J. Appl. Phys.* **121**, 103903, doi:10.1063/1.4978315 (2017).

111 Sklenar, J., Bhat, V. S., DeLong, L. E. & Ketterson, J. B. Broadband ferromagnetic resonance studies on an artificial square spin-ice island array. *J. Appl. Phys.* **113**, 17B530, doi:10.1063/1.4800740 (2013).

112 Ma, F., Wu, Y. & Zong, B. Micromagnetic Investigation of Microwave Permeability of Magnetic Artificial Spin Ice. *Mater. Sci. Appl.* **05**, 991, doi:10.4236/msa.2014.514100 (2014).

113 Montoncello, F. *et al.* Mutual influence between macrospin reversal order and spin-wave dynamics in isolated artificial spin-ice vertices. *Phys. Rev. B* **97**, 014421, doi:10.1103/PhysRevB.97.014421 (2018).

114 Mironov, V. L., Skorohodov, E. V. & Blackman, J. A. Magnetic states and ferromagnetic resonance in geometrically frustrated arrays of multilayer ferromagnetic nanoparticles ordered on triangular lattices. *J. Appl. Phys.* **115**, 184301, doi:10.1063/1.4875479 (2014).

115 Gliga, S., Kákay, A., Heyderman, L. J., Hertel, R. & Heinonen, O. G. Broken vertex symmetry and finite zero-point entropy in the artificial square ice ground state. *Phys. Rev. B* **92**, 060413, doi:10.1103/PhysRevB.92.060413 (2015).

116 Behncke, C. *et al.* Tunable geometrical frustration in magnonic vortex crystals. *Sci. Rep.* **8**, 186, doi:10.1038/s41598-017-17480-1 (2018).

117 Jungfleisch, M. B. *et al.* High-Frequency Dynamics Modulated by Collective Magnetization Reversal in Artificial Spin Ice. *Phys. Rev. Applied* **8**, 064026, doi:10.1103/PhysRevApplied.8.064026 (2017).

118 Bhat, V. S. & Grundler, D. Angle-dependent magnetization dynamics with mirror-symmetric excitations in artificial quasicrystalline nanomagnet lattices. *Phys. Rev. B* **98**, 174408, doi:10.1103/PhysRevB.98.174408 (2018).

119 Kruglyak, V. V. *et al.* Formation of the band spectrum of spin waves in 1D magnonic crystals with different types of interfacial boundary conditions. *J. Phys. D: Appl. Phys.* **50**, 094003, doi:10.1088/1361-6463/aa536c (2017).

120 Szulc, K. *et al.* Remagnetization in arrays of ferromagnetic nanostripes with periodic and quasiperiodic order. *Phys. Rev. B* **99**, 064412, doi:10.1103/PhysRevB.99.064412 (2019).

121 Lisiecki, F. *et al.* Reprogrammability and Scalability of Magnonic Fibonacci Quasicrystals. *Phys. Rev. Applied* **11**, 054003, doi:10.1103/PhysRevApplied.11.054003 (2019).

122 Iacocca, E., Gliga, S., Stamps, R. L. & Heinonen, O. Reconfigurable wave band structure of an artificial square ice. *Phys. Rev. B* **93**, 134420, doi:10.1103/PhysRevB.93.134420 (2016).

123 Iacocca, E. & Heinonen, O. Topologically Nontrivial Magnon Bands in Artificial Square Spin Ices with Dzyaloshinskii-Moriya Interaction. *Phys. Rev. Applied* **8**, 034015, doi:10.1103/PhysRevApplied.8.034015 (2017).

124 Zhou, X., Chua, G. L., Singh, N. & Adeyeye Adekunle, O. Large Area Artificial Spin Ice and Anti-Spin Ice $Ni_{80}Fe_{20}$ Structures: Static and Dynamic Behavior. *Adv. Funct. Mater.* **26**, 1437-1444, doi:10.1002/adfm.201505165 (2016).

125 Schneider, T. *et al.* Programmability of Co-antidot lattices of optimized geometry. *Sci. Rep.* **7**, 41157, doi:10.1038/srep41157 (2017).

126 Mamica, S., Krawczyk, M. & Grundler, D. Nonuniform Spin-Wave Softening in Two-Dimensional Magnonic Crystals as a Tool for Opening Omnidirectional Magnonic Band Gaps. *Phys. Rev. Applied* **11**, 054011, doi:10.1103/PhysRevApplied.11.054011 (2019).

127 Mamica, S., Zhou, X., Adeyeye, A., Krawczyk, M. & Gubbiotti, G. Spin-wave dynamics in artificial anti-spin-ice systems: Experimental and theoretical investigations. *Phys. Rev. B* **98**, 054405, doi:10.1103/PhysRevB.98.054405 (2018).

128 Grundler, D. Nanomagnonics. *J. Phys. D: Appl. Phys.* **49**, 391002, doi:10.1088/0022-3727/49/39/391002 (2016).

129 Li, J. *et al.* Comparing artificial frustrated magnets by tuning the symmetry of nanoscale permalloy arrays. *Phys. Rev. B* **81**, 092406, doi:10.1103/PhysRevB.81.092406 (2010).

130 Farhan, A. *et al.* Nanoscale control of competing interactions and geometrical frustration in a dipolar trident lattice. *Nat. Commun.* **8**, 995, doi:10.1038/s41467-017-01238-4 (2017).

131 Macêdo, R., Macauley, G. M., Nascimento, F. S. & Stamps, R. L. Apparent ferromagnetism in the pinwheel artificial spin ice. *Phys. Rev. B* **98**, 014437, doi:10.1103/PhysRevB.98.014437 (2018).

132 Li, Y. *et al.* Superferromagnetism and domain-wall topologies in artificial 'pinwheel' spin ice. *ACS Nano* **13**, 2213-2222, doi:10.1021/acsnano.8b08884 (2019).

133 Yu, L. *et al.* Monte Carlo simulation on a new artificial spin ice lattice consisting of hexagons and three-moment vertices. *AIP Advances* **7**, 085211, doi:10.1063/1.4995588 (2017).

134 Lehmann, J., Donnelly, C., Derlet, P. M., Heyderman, L. J. & Fiebig, M. Poling of an artificial magneto-toroidal crystal. *Nat. Nanotechnol.* **14**, 141-144, doi:10.1038/s41565-018-0321-x (2018).

135 Wang, Y.-L. *et al.* Rewritable artificial magnetic charge ice. *Science* **352**, 962-966, doi:10.1126/science.aad8037 (2016).

136 Chern, G.-W., Morrison, M. J. & Nisoli, C. Degeneracy and Criticality from Emergent Frustration in Artificial Spin Ice. *Phys. Rev. Lett.* **111**, 177201, doi:10.1103/PhysRevLett.111.177201 (2013).

137 Stopfel, H. *et al.* Magnetic order and energy-scale hierarchy in artificial spin-ice structures. *Phys. Rev. B* **98**, 014435, doi:10.1103/PhysRevB.98.014435 (2018).

138 Mydosh, J. A. *Spin Glasses: An Experimental Introduction*. (Taylor & Francis, 1993).

139 Saccone, M. *et al.* Towards artificial Ising spin glasses: Thermal ordering in randomized arrays of Ising-type nanomagnets. *Phys. Rev. B* **99**, 224403, doi:10.1103/PhysRevB.99.224403 (2019).

140 Islam, Z. *et al.* Reinvestigation of long-range magnetic ordering in icosahedral Tb-Mg-Zn. *Phys. Rev. B* **57**, R11047-R11050, doi:10.1103/PhysRevB.57.R11047 (1998).

141 Chernikov, M. A., Bernasconi, A., Beeli, C., Schilling, A. & Ott, H. R. Low-temperature magnetism in icosahedral $Al_{70}Mn_{9}Pd_{21}$. *Phys. Rev. B* **48**, 3058-3065, doi:10.1103/PhysRevB.48.3058 (1993).

142 Penrose, R. Role of aesthetics in pure and applied mathematical research. *Bull. Inst. Math. & Appl.* **10** (1974).

143 Vedmedenko, E. Y., Oepen, H. P. & Kirschner, J. Decagonal Quasiferromagnetic Microstructure on the Penrose Tiling. *Phys. Rev. Lett.* **90**, 137203, doi:10.1103/PhysRevLett.90.137203 (2003).

144 Vedmedenko, E. Y., Grimm, U. & Wiesendanger, R. Interplay between magnetic and spatial order in quasicrystals. *Philosoph. Mag.* **86**, 733-739, doi:10.1080/14786430500363569 (2006).

145 Bhat, V. S. *et al.* Controlled Magnetic Reversal in Permalloy Films Patterned into Artificial Quasicrystals. *Phys. Rev. Lett.* **111**, 077201, doi:10.1103/PhysRevLett.111.077201 (2013).

146 Brajuskovic, V., Barrows, F., Phatak, C. & Petford-Long, A. K. Real-space observation of magnetic excitations and avalanche behavior in artificial quasicrystal lattices. *Sci. Rep.* **6**, 34384, doi:10.1038/srep34384 (2016).

147 Brajuskovic, V., Addi, A., Phatak, C. & Petford-Long, A. K. Observation of transient states during magnetization reversal in a quasicrystal artificial spin ice. *Phys. Rev. B* **98**, 094424, doi:10.1103/PhysRevB.98.094424 (2018).

148 Barrows, F., Brajuskovic, V., Petford-Long, A. K. & Phatak, C. Emergent magnetic ordering and topological frustration in quasicrystal artificial spin ices. *Phys. Rev. B* **99**, 094424, doi:10.1103/PhysRevB.99.094424 (2019).

149 Nisoli, C. in *Frustrated Materials and Ferroic Glasses* (eds Turab Lookman & Xiaobing Ren) 57-99 (Springer International Publishing, 2018).

150 Stamps, R. L. Artificial spin ice: The unhappy wanderer. *Nat. Phys.* **10**, 623-624, doi:10.1038/nphys3072 (2014).

151 Perron, J. *et al.* Extended reciprocal space observation of artificial spin ice with x-ray resonant magnetic scattering. *Phys. Rev. B* **88**, 214424, doi:10.1103/PhysRevB.88.214424 (2013).

152 Lee, J. C. T. *et al.* Textured heterogeneity in square artificial spin ice. *Phys. Rev. B* **99**, 024406, doi:10.1103/PhysRevB.99.024406 (2019).

153 Mistonov, A. A. *et al.* Magnetic structure of the inverse opal-like structures: small angle neutron diffraction and micromagnetic simulations. *J. Magn. Magn. Mater.* **477**, 99-108, doi:10.1016/j.jmmm.2019.01.016 (2019).

154 Chen, X. M. *et al.* Spontaneous Magnetic Superdomain Wall Fluctuations in an Artificial Antiferromagnet. *arXiv:1809.05656 [cond-mat]* (2018).

155 Santos-Filho, J. B., Plascak, J. A., Sobrinho, M. C. & Araujo Batista, T. S. Phase diagram of the XY Vector Blume–Emery–Griffiths model on a Kagome lattice by Monte Carlo simulation. *Physica A* **503**, 844-848, doi:10.1016/j.physa.2018.03.020 (2018).

156 Streubel, R. *et al.* Magnetism in curved geometries. *J. Phys. D: Appl. Phys.* **49**, 363001, doi:10.1088/0022-3727/49/36/363001 (2016).

157 Fernández-Pacheco, A. *et al.* Three-dimensional nanomagnetism. *Nat. Commun.* **8**, 15756, doi:10.1038/ncomms15756 (2017).

158 Lavrijsen, R. *et al.* Magnetic ratchet for three-dimensional spintronic memory and logic. *Nature* **493**, 647-650, doi:10.1038/nature11733 (2013).

159 Kadic, M., Bückmann, T., Stenger, N., Thiel, M. & Wegener, M. On the practicability of pentamode mechanical metamaterials. *Appl. Phys. Lett.* **100**, 191901, doi:10.1063/1.4709436 (2012).

160 Williams, G. *et al.* Two-photon lithography for 3D magnetic nanostructure fabrication. *Nano Res.* **11**, 845-854, doi:10.1007/s12274-017-1694-0 (2018).

161 May, A., Hunt, M., Berg, A. V. D., Hejazi, A. & Ladak, S. Realisation of a frustrated 3D magnetic nanowire lattice. *Commun. Phys.* **2**, 13, doi:10.1038/s42005-018-0104-6 (2019).

162 Donnelly, C. *et al.* Element-Specific X-Ray Phase Tomography of 3D Structures at the Nanoscale. *Phys. Rev. Lett.* **114**, 115501, doi:10.1103/PhysRevLett.114.115501 (2015).

163 Frenzel, T., Kadic, M. & Wegener, M. Three-dimensional mechanical metamaterials with a twist. *Science* **358**, 1072-1074, doi:10.1126/science.aao4640 (2017).

164 Keller, L. *et al.* Direct-write of free-form building blocks for artificial magnetic 3D lattices. *Sci. Rep.* **8**, 6160, doi:10.1038/s41598-018-24431-x (2018).

165 Fowlkes, J. D. *et al.* High-Fidelity 3D-Nanoprinting via Focused Electron Beams: Computer-Aided Design (3BID). *ACS Appl. Nano Mater.* **1**, 1028-1041, doi:10.1021/acsanm.7b00342 (2018).

166 Mistonov, A. A. *et al.* Three-dimensional artificial spin ice in nanostructured Co on an inverse opal-like lattice. *Phys. Rev. B* **87**, 220408, doi:10.1103/PhysRevB.87.220408 (2013).

167 Shishkin, I. S. *et al.* Nonlinear geometric scaling of coercivity in a three-dimensional nanoscale analog of spin ice. *Phys. Rev. B* **94**, 064424, doi:10.1103/PhysRevB.94.064424 (2016).

168 Chopdekar, R. V. *et al.* Nanostructured complex oxides as a route towards thermal behavior in artificial spin ice systems. *Phys. Rev. Materials* **1**, 024401, doi:10.1103/PhysRevMaterials.1.024401 (2017).

169 Cowburn, R. P. Property variation with shape in magnetic nanoelements. *J. Phys. D: Appl. Phys.* **33**, R1, doi:10.1088/0022-3727/33/1/201 (2000).

170 Wang, Y.-L. *et al.* Switchable geometric frustration in an artificial-spin-ice–superconductor heterosystem. *Nat. Nanotechnol.* **13**, 560-565, doi:10.1038/s41565-018-0162-7 (2018).

171 Rollano, V. *et al.* Topologically protected superconducting ratchet effect generated by spin-ice nanomagnets. *Nanotechnology* **30**, 244003, doi:10.1088/1361-6528/ab0923 (2019).

172 Torrejon, J. *et al.* Neuromorphic computing with nanoscale spintronic oscillators. *Nature* **547**, 428-431, doi:10.1038/nature23011 (2017).

173 Luo, Z. *et al.* Chirally coupled nanomagnets. *Science* **363**, 1435-1439, doi:10.1126/science.aau7913 (2019).

174 Le, B. L. *et al.* Understanding magnetotransport signatures in networks of connected permalloy nanowires. *Phys. Rev. B* **95**, 060405, doi:10.1103/PhysRevB.95.060405 (2017).

175 Gypens, P., Leliaert, J. & Van Waeyenberge, B. Balanced Magnetic Logic Gates in a Kagome Spin Ice. *Phys. Rev. Applied* **9**, 034004, doi:10.1103/PhysRevApplied.9.034004 (2018).

176 Caravelli, F. & Nisoli, C. Computation via Interacting Magnetic Memory Bites: Integration of Boolean Gates. *arXiv:1810.09190 [cond-mat.dis-nn]* (2018).

177 Arava, H. *et al.* Engineering Relaxation Pathways in Building Blocks of Artificial Spin Ice for Computation. *Phys. Rev. Applied* **11**, 054086, doi:10.1103/PhysRevApplied.11.054086 (2019).

178 Arava, H. *et al.* Computational logic with square rings of nanomagnets. *Nanotechnology* **29**, 265205, doi:10.1088/1361-6528/aabbc3 (2018).

179 Pan, L., Laurita, N. J., Ross, K. A., Gaulin, B. D. & Armitage, N. P. A measure of monopole inertia in the quantum spin ice $Yb_2Ti_2O_7$. *Nat. Phys.* **12**, 361-366, doi:10.1038/nphys3608 (2016).

180 Li, Z. *et al.* Simultaneous Local Heating/Thermometry Based on Plasmonic Magnetochromic Nanoheaters. *Small* **14**, 1800868, doi:10.1002/smll.201800868 (2018).

181 Pancaldi, M., Leo, N. & Vavassori, P. Selective and fast plasmon-assisted photo-heating of nanomagnets. *Nanoscale* **11**, 7656-7666, doi:10.1039/C9NR01628G (2019).

182 Khajetoorians, A. A. *et al.* Atom-by-atom engineering and magnetometry of tailored nanomagnets. *Nat. Phys.* **8**, 497-503, doi:10.1038/nphys2299 (2012).

183 Hong, J., Lambson, B., Dhuey, S. & Bokor, J. Experimental test of Landauer's principle in single-bit operations on nanomagnetic memory bits. *Sci. Adv.* **2**, e1501492, doi:10.1126/sciadv.1501492 (2016).

184 Libál, A., Reichhardt, C. & Reichhardt, C. J. O. Realizing Colloidal Artificial Ice on Arrays of Optical Traps. *Phys. Rev. Lett.* **97**, 228302, doi:10.1103/PhysRevLett.97.228302 (2006).

185 Libál, A. *et al.* Ice rule fragility via topological charge transfer in artificial colloidal ice. *Nat. Commun.* **9**, 4146, doi:10.1038/s41467-018-06631-1 (2018).

186 Han, Y. *et al.* Geometric frustration in buckled colloidal monolayers. *Nature* **456**, 898-903, doi:10.1038/nature07595 (2008).

187 Le Cunuder, A., Frérot, I., Ortiz-Ambriz, A. & Tierno, P. Competing orders in colloidal kagome ice: Importance of the in-trap motion of the particles. *Phys. Rev. B* **99**, 140405, doi:10.1103/PhysRevB.99.140405 (2019).

188 Libál, A., Reichhardt, C. J. O. & Reichhardt, C. Creating Artificial Ice States Using Vortices in Nanostructured Superconductors. *Phys. Rev. Lett.* **102**, 237004, doi:10.1103/PhysRevLett.102.237004 (2009).

189 Xue, C. *et al.* Tunable artificial vortex ice in nanostructured superconductors with a frustrated kagome lattice of paired antidots. *Phys. Rev. B* **97**, 134506, doi:10.1103/PhysRevB.97.134506 (2018).

190 Kang, S. H. *et al.* Complex Ordered Patterns in Mechanical Instability Induced Geometrically Frustrated Triangular Cellular Structures. *Phys. Rev. Lett.* **112**, 098701, doi:10.1103/PhysRevLett.112.098701 (2014).

191 Nisoli, C. Unexpected Phenomenology in Particle-Based Ice Absent in Magnetic Spin Ice. *Phys. Rev. Lett.* **120**, 167205, doi:10.1103/PhysRevLett.120.167205 (2018).

192 Conde-Rubio, A. *et al.* Geometric frustration in a hexagonal lattice of plasmonic nanoelements. *Opt. Express, OE* **26**, 20211-20224, doi:10.1364/OE.26.020211 (2018).

193 Gunnarsson, K. *et al.* Programmable Motion and Separation of Single Magnetic Particles on Patterned Magnetic Surfaces. *Adv. Mater.* **17**, 1730-1734, doi:10.1002/adma.200401880 (2005).

194 Fert, A., Cros, V. & Sampaio, J. Skyrmions on the track. *Nat. Nanotechnol.* **8**, 152-156, doi:10.1038/nnano.2013.29 (2013).

195 Ma, F., Reichhardt, C., Gan, W., Reichhardt, C. J. O. & Lew, W. S. Emergent geometric frustration of artificial magnetic skyrmion crystals. *Phys. Rev. B* **94**, 144405, doi:10.1103/PhysRevB.94.144405 (2016).

196 Braun, H.-B. Topological effects in nanomagnetism: from superparamagnetism to chiral quantum solitons. *Advances in Physics* **61**, 1-116, doi:10.1080/00018732.2012.663070 (2012).

197 Ryzhkin, I. A. Magnetic relaxation in rare-earth oxide pyrochlores. *J. Exp. Theor. Phys.* **101**, 481-486, doi:10.1134/1.2103216 (2005).

198 Pohle, R., Benton, O. & Jaubert, L. D. C. Reentrance of disorder in the anisotropic shuriken Ising model. *Phys. Rev. B* **94**, 014429, doi:10.1103/PhysRevB.94.014429 (2016).

199 Arnalds, U. B. *et al.* A new look on the two-dimensional Ising model: thermal artificial spins. *New J. Phys.* **18**, 023008, doi:10.1088/1367-2630/18/2/023008 (2016).

200 Chioar, I. A., Rougemaille, N. & Canals, B. Ground-state candidate for the classical dipolar kagome Ising antiferromagnet. *Phys. Rev. B* **93**, 214410, doi:10.1103/PhysRevB.93.214410 (2016).

201 Zhang, S. *et al.* Perpendicular Magnetization and Generic Realization of the Ising Model in Artificial Spin Ice. *Phys. Rev. Lett.* **109**, 087201, doi:10.1103/PhysRevLett.109.087201 (2012).

202 Park, J. *et al.* Magnetic response of brickwork artificial spin ice. *Phys. Rev. B* **96**, 024436, doi:10.1103/PhysRevB.96.024436 (2017).

203 Liu, Y. *et al.* Confined Chemical Fluid Deposition of Ferromagnetic Metalattices. *Nano Lett.* **18**, 546-552, doi:10.1021/acs.nanolett.7b04633 (2018).